




Geochemistry of mafic–ultramafic magmatism in the Western Ghats belt (Kudremukh greenstone belt), western Dharwar Craton, India: implications for mantle sources and geodynamic setting

Chandan-Kumar B & A. G. Ugarkar


To cite this article: Chandan-Kumar B & A. G. Ugarkar (2017) Geochemistry of mafic–ultramafic magmatism in the Western Ghats belt (Kudremukh greenstone belt), western Dharwar Craton, India: implications for mantle sources and geodynamic setting, International Geology Review, 59:12, 1507-1531, DOI: [10.1080/00206814.2017.1278623](https://doi.org/10.1080/00206814.2017.1278623)

To link to this article: <https://doi.org/10.1080/00206814.2017.1278623>

 View supplementary material [↗](#)

 Published online: 27 Jan 2017.

 Submit your article to this journal [↗](#)

 Article views: 334

 View related articles [↗](#)

 View Crossmark data [↗](#)

 Citing articles: 10 View citing articles [↗](#)

ARTICLE



Geochemistry of mafic–ultramafic magmatism in the Western Ghats belt (Kudremukh greenstone belt), western Dharwar Craton, India: implications for mantle sources and geodynamic setting

Chandan-Kumar B ^{a,b} and A. G. Ugarkar^a

^aDepartment of Studies in Geology, Karnatak University, Dharwad, India; ^bDepartment of Geology, Central University of Kerala, Kasaragod, India

ABSTRACT

Western Ghats Belt of western Dharwar Craton is dominated by metavolcanic rocks (komatiites, high-magnesium basalts (HMBs), basalts, boninites) with occasional metagabbros. This rock-suite has undergone post-magmatic alteration processes corresponding to greenschist- to lower-amphibolite facies conditions. Komatiites are Al-depleted, characterized by lower Al_2O_3/TiO_2 and high CaO/Al_2O_3 . Their trace element distribution patterns suggest most of the primary geochemical compositions are preserved with minor influence of post-magmatic alteration processes and negligible crustal contamination. Chemical characteristics of Al-depleted komatiites imply their derivation from deeper upper mantle with/without garnet involvement. HMBs and basalts are differentiated based on their magnesium content. Basalts and occasionally associated gabbroic sills have similar geochemical characteristics. HMB are characterized by light rare earth element (LREE) enrichment, with significant Nb–Ta and Zr negative anomalies. Basalts and associated gabbros display tholeiitic affinity, with LREE-enriched to slightly fractionated heavy rare earth element (HREE) patterns. Boninites are distinctive in conjunction of low abundances of incompatible elements with respect to the studied komatiites. Chondrite-normalized REE patterns of boninites show relative enrichment in LREE and HREE with respect to MREE. Prominent island arc signatures are evident in HMB, basalts, boninites, and gabbros in terms of their Nb–Ta and Zr–Hf negative anomalies, LREE enrichment and HFSE depletion. It is suggested that these HMB–basalts (associated gabbros)–boninites are the products of arc magmatism. Their REE chemistry attests to a gradual transition in melting depth varying between spinel and garnet stability field in an arc regime. The close spatial association but contrasting elemental characteristics of komatiites and HMB–basalts–boninites can be explained by a plume-arc model, in which the ~3.0 Ga komatiites are considered to be the products of plume volcanism in an oceanic setting, while the HMB, basalts, boninites, and associated gabbros were emplaced in a continental margin setting around 2.8–2.7 Ga.

ARTICLE HISTORY

Received 22 September 2016
Accepted 1 January 2017


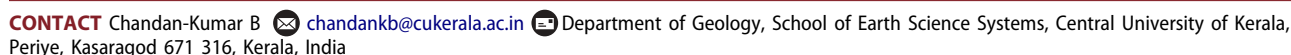
KEYWORDS


Western Ghats belt;
Kudremukh belt; komatiites;
boninites; mantle sources;
greenstone belts

1. Introduction

The origin of Archaean greenstone belts is a matter of long-standing debate (Condie 1981; Kröner 1991; Windley 1993; Dostal *et al.* 2004; Benn *et al.* 2013; Dey *et al.* 2013; Lancaster *et al.* 2015). Two different approaches have been established to explain the origin of these greenstone belts, viz. uniformitarian plate tectonic and non-uniformitarian non-plate tectonic fixist approaches (see Condie 1981; Polat *et al.* 1998; for reviews). Rock associations that were characteristic of Archaean magma generation process such as plume-related tholeiitic basalt–komatiitic–chert–greywacke association and arc-related basalt–Nb-enriched basalt–boninite–adakite–high Mg andesite association of

superior craton are recognized in modern geodynamic setting (Dey *et al.* 2013 and references therein). Similarly, modern-style geodynamic processes such as plume-subduction/lithosphere interaction, subduction accretion, thrusting and imbrication, strike-slip faulting, continental rifting and orogenic collapse have been reported from Archaean Cratonic areas, viz. Greenland, Tanzania, Pilbara, and Karelian Cratons (Dey *et al.* 2013 and references therein). Similar geodynamic process have also been reported from Archaean Dharwar Craton (DC) in the past three decades (Drury 1983; Chardon *et al.* 2008, 2011; Jayananda *et al.* 2008; Manikyamba and Kerrich 2012; Manikyamba *et al.* 2012).

CONTACT Chandan-Kumar B  chandankb@cukerala.ac.in 

 Supplemental data for this article can be accessed [here](#).

© 2017 Informa UK Limited, trading as Taylor & Francis Group

Ramakrishnan and Vaidyanadhan (2010) have recorded several cycles of supracrustal development, deformation, metamorphism and granitic intrusion from the DC. This South Indian Craton hosts numerous early to late Archaean greenstone belts and, therefore, is one of the ideal terranes for understanding the nature of Archaean geodynamics and crustal evolution. The craton has been extensively studied for more than a century since the historical work of Bruce Foote (1886) and pioneering field studies by geologists of the Mysore Geological Department (MGD) (cf. Ramachandra 2016). For the past one decade, voluminous geochemical, isotopic, and geochronological data have been generated on the craton and have been interpreted in terms of modern plate and plume concepts (Chadwick *et al.* 2007, 2003; Jayananda *et al.* 2013a, 2008; Peucat *et al.* 2013a; Ugarkar *et al.* 2014; references therein). Komatiite volcanism has been extensively studied in the DC since the first report by Viswanatha *et al.* (1977) from Ghattihosahalli schist belt of western DC (WDC). Since then many occurrences of komatiites have been reported from the western and eastern DC (EDC) (Iyer and Vasudev 1979; Rajamani *et al.* 1985; Srikantia and Bose 1985; Charan *et al.* 1988; Srikantia and Venkataramana 1989; Jafri *et al.* 1997; Rao and Naqvi 1999; Naqvi *et al.* 2002; Manikyamba *et al.* 2007; Jayananda *et al.* 2008; Ugarkar *et al.* 2014). Jayananda *et al.* (2008) in their landmark study on the Palaeoarchaeoan Sargur Group komatiites proposed for the first time a plume-arc model for the widespread 3.35 Ga komatiite volcanism and sub-contemporaneous granitoid plutonism in the WDC. Manikyamba *et al.* (2005) reported boninites for the first time from Gadwal greenstone belt of EDC. They reported higher geothermal gradient and variable fluid flux in 2.7 Ga old subduction zone as a possible mechanism for the generation of Gadwal greenstone belt in the EDC. This study led to the further discoveries of boninites from western and eastern DC (Naqvi *et al.* 2006; Ganguly *et al.* 2016).

In spite of this enormous work in the DC, what is known so far about the low-high grade Western Ghats belt (WGB; popularly known as Kudremukh Greenstone Belt in the literatures) in the WDC (Sampat Iyengar 1912; Ramakrishnan and Harinadha Babu 1981), is very little. Though the belt is approximately 150 km long, 25 km wide, and covers an area of about 7500 km² with a vast resources of magnetic iron ore, it is not completely explored in the past due to limited accessibility. The WGB, consisting of volcano-sedimentary sequences of older Sargur Group (>3.2 Ga) and younger Dharwar Supergroup (2.9–2.5 Ga), rests unconformably upon the Palaeo–Mesoarchaeoan gneissic complex. Previously

it was thought that the schistose rocks of WGB encompassed three discontinuous and independent belts, viz. Kudremukh, Agumbe, and Kodachadri, separated by gneisses occurring in between (Rama Rao 1962). Accordingly, WGB to the south of Agumbe region was referred as Kudremukh greenstone belt in earlier literatures. However, it was found later that these three belts were continuous (Ramakrishnan and Harinadha Babu 1981).

Most of the published geochemical work so far in the WGB corresponds to the metavolcanics and banded iron formations (BIF) of Kudremukh region (Drury 1981; Khan *et al.* 1992, 1995) while the geochronological work corresponds to the metavolcanics of Kudremukh region and the basement gneisses (Balasubramanyam 1978; Balasubramanyam *et al.* 1982; Drury *et al.* 1983). Drury (1981) reported the metabasalts of Kudremukh region and its surrounding area as low K-tholeiites based on their geochemistry. Occasional metaperidotites were also reported from the same locality (Drury 1981). Balasubramanyam (1978) reported that the basement gneisses were 3550–3180 million years old based on K/Ar ages of biotite from the gneisses. However, there are no data on the geochemical characteristics, magmatic history including post-magmatic alteration processes, composition of mantle sources and geodynamic history of the metavolcanics and the associated plutons of the Agumbe and Kodachadri sections of WGB, which forms a continuous belt along with the Kudremukh section.

Many geodynamic and crustal evolution models for DC have been proposed so far (see Jayananda *et al.* 2013b, 2015). But, all these models are constructed based on the available data from the well-documented greenstone belts of DC. Proper consideration to WGB is not given in these models due to scarcity of high precision geochemical and isotopic data. Any attempt to model a tectonic and crustal growth process in the DC would be futile, if all the existing greenstone belts and their mutual relationship, and with that of basement rocks (granitic/gneissic) are not taken into consideration. Consequently, the main purpose of this article is to present the petrographic and geochemical data for the metavolcanics and associated mafic plutons of the entire WGB in order to discuss their genesis and tectonic evolution.

2. Regional geology

DC (Figure 1(a)), one among the five Archaean Cratons in India, preserves an essentially complete geological record from 3.5 to 2.5 Ga, making it one of the best terrains in the world to study Palaeo–Neoarchaeoan

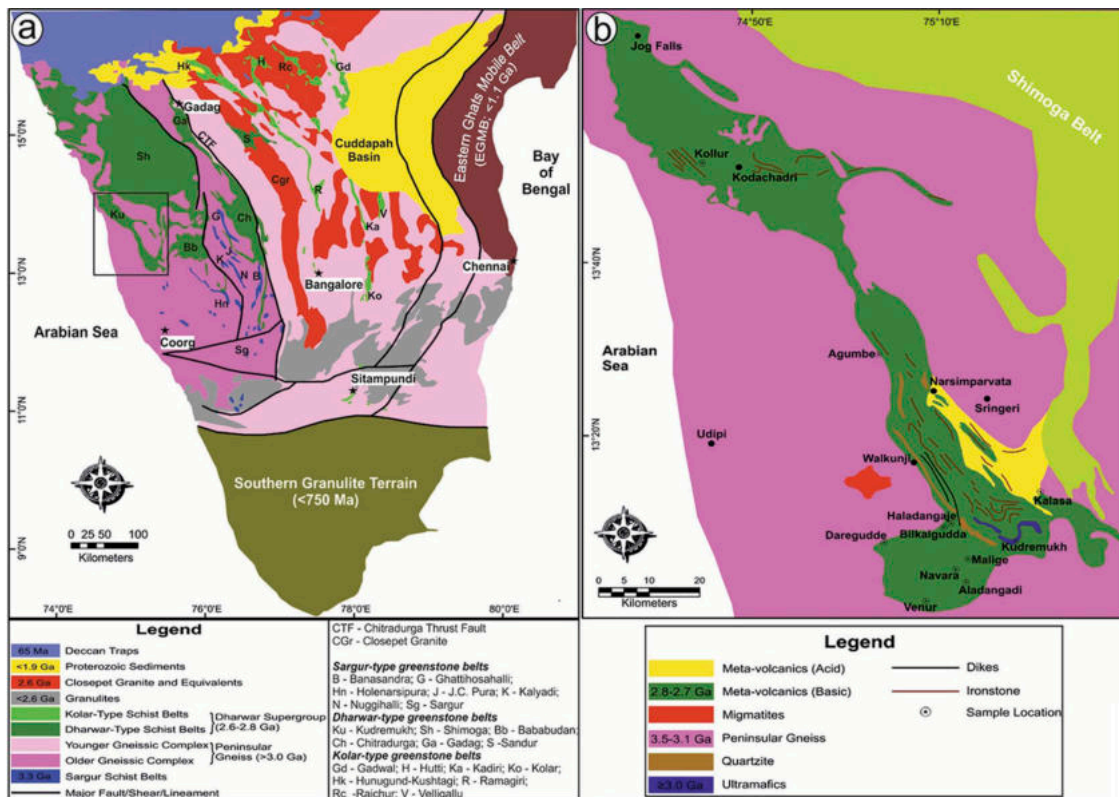


Figure 1. (a) Geological map of Dharwar Craton (after Devaraju et al. (2009)). (b) Geological map of Western Ghats (Kudremukh) belt (modified after Ramakrishnan and Harinadha Babu 1981).

geodynamics, mantle chemistry and crustal evolution. The vast expanse of DC is divisible into two, the WDC and the EDC, the boundary between the two being considered to be marked either by the regional ductile shear zone (CSZ – Chitradurga Shear Zone) on the eastern margin of the Chitradurga Schist Belt, or by the Closepet Granite (see Ramachandra 2016). Distinct geodynamic settings are reported for the volcano-sedimentary associations in the schist belts of WDC and EDC, which is evident through recent petrological and geochemical studies (Balakrishnan et al. 1999; Manikyamba and Kerrich 2011; Ugarkar et al. 2013, 2014, 2016; Jayananda et al. 2013a, 2015; Manikyamba et al. 2014). Recently, based on combined U–Pb zircon ages and Nd isotope data, the craton has been divided into three provinces western (dominated by 3.4–3.2 Ga crust), central (mixed older 3.4–3.2 Ga and younger 2.7–2.52 Ga crust), and eastern (dominated by 2.7–2.52 Ga crust without significant crustal remnants older than 2.7 Ga) (Peucat et al. 2013; Jayananda et al. 2013b).

The WDC is dominated by older basement TTG (>3.2 Ga), with interlayered Sargur Group greenstone belts, unconformably overlain by 2.9–2.7 Ga Dharwar Supergroup volcano-sedimentary greenstone belts (Swami Nath and Ramakrishnan 1981; Peucat et al. 1993; Nutman et al. 1996; Jayananda et al. 2008,

2013b). The Dharwar Supergroup is divided into a lower Bababudan Group and an upper Chitradurga Group (Swami Nath and Ramakrishnan 1981). The EDC comprises younger (2.7–2.6 Ga) grey tonalitic gneisses with large remnants of 3.0–3.32 Ga TTG (Krogstad et al. 1991; Peucat et al. 1993; Balakrishnan et al. 1999; Jayananda et al. 2000; Chardon et al. 2002), thin elongated 2.7–2.56 Ga volcanic dominated gold bearing schist belts of Kolar Group and diamondiferous kimberlites (Swami Nath et al. 1976; Balakrishnan et al. 1991; Chalapathi Rao et al. 2013). The whole Archaean crust in the DC was affected by at least four major tectonothermal events at 3.24, 3.1–3.0, 2.62, and 2.51–2.45 Ga (Peucat et al. 1993, 2013; Jayananda et al. 2011, 2013b). The craton corresponds to a large tilted oblique section of the Archaean continental crust, and generally, from north to south within the craton there is a progressive increase in the grade of metamorphism from greenschist to granulite facies (Chadwick et al. 2000).

3. WGB (Kudremukh belt)

WGB extends from Kudremukh in the south to Jog Falls in the north through Agumbe and Kodachadri peaks (Figure 1(b)). Further north it passes into Shimoga belt beyond Sharavathi River up to Goa. WGB is surrounded

by 3.3 Ga old TTG to the south and west, and in the east, it is separated from the neighbouring Shimoga belt by the gneisses occurring in between. The stratigraphic succession of the Dharwar Supergroup (2.8–2.6 Ga) of rocks in the WGB has been divided into Walkunje, Kudremukh, Kodachadri, and Narsiparvata Formations, and is similar to that of Bababudan greenstone belt (Table 1; Ramakrishnan and Harinadha Babu 1981). The basal bed resting unconformably over the basement gneiss is the oligomict quartz-pebble conglomerate (Walkunje Conglomerate of *Walkunje Formation*) with associated cross-bedded quartzite. The conglomerate is mineralogically and texturally similar to Kartikere Conglomerate of Bababudan belt, and are associated with quartzites, quartz-sericite schist, arkose, and quartz-chlorite-biotite schist. These conglomerates are overlain by thick sequence of metamorphosed basic volcanics with minor intercalations of metasediments of *Kudremukh Formation* suggesting a number of flows with intervening periods of sedimentation. Metabasalts and associated metagabbroic sills, actinolite-chlorite schists and ultramafics form part of the metamorphosed basic lithologies of this formation. The litho units of *Kudremukh Formation* are considered to be equivalents

(?) of Santevari Formation (~2.7 Ga) of Bababudan belt (Ramakrishnan and Harinadha Babu 1981). A major unit of Algoma-type BIF, belonging to *Kodachadri Formation*, caps the Aroli hills of Kudremukh area, and the Kodachadri hills. These BIFs are considered to be equivalents of Mulaingiri Formation of Bababudan belt. They contain rare seams of amosite asbestos and local layers rich in alkali amphibole (Ramakrishnan and Vaidyanadhan 2010). The BIF is overlain by a major horizon of basalts, chloritic phyllites, felsic volcanics, and pyroclastics which belong to *Narsiparvata Formation* and are typically exposed in Narasimhaparvatha Hills. These correspond to the Jagar Formation of Bababudan Belt (Ramakrishnan and Vaidyanadhan 2010).

The contact between the basement gneiss and the greenstones (Dharwar Supergroup of rocks) is in many places sharp, but at places it is sheared and, hence, indicates tectonic contact. The grade of metamorphism in WGB varies from amphibolite facies on basal sequence (periphery of the belt) and greenschist facies in the upper formations (core of the belt). The variation in metamorphic grade form the margins towards the core of the belt is one of the characteristic features of

Table 1. Tectonostratigraphic elements of the Bababudan and Western Ghats (Kudremukh) belt (modified after Ramakrishnan and Harinadha Babu 1981).

Dharwar Supergroup (2600–2800 Ma)	Bababudan Belt		Western Ghat (Kudremukh) Belt	
	Chitradurga Group	Jagar formation (Ingaldhal formation of Vanivilas subgroup)	Mafic-felsic volcanics with BIF, phyllites	Narsiparvata section (Ingaldhal formation of Vanivilas subgroup)
-----Disconformity-----				
Bababudan Group	Mulaingiri formation	BIF with phyllites and rare ultramafic-mafic sills	Kodachadri formation	Algoma-type BIF (oxide and silicate facies, with minor carbonate facies)
	Santevari formation	Metabasalts, felsic volcanics (Galipuje felsite), ultramafic schists, layered basic complexes, siliceous phyllites, cross-bedded quartzite (Kaimara, Tanigebail)	Kudremukh formation	Metabasalts with rare agglomerates, ultramafic schists quartzites phyllites and minor BIF, dolomitized limestones
	Allampura formation	Metabasalts, gabbros, ultramafic schists, local BIF, phyllites, cross-bedded quartzite (Lakya)		
	Kalasapura formation	Metabasalts, gabbros, ultramafic schists, phyllites, quartzites, basal quartz pebble conglomerate (Kartikere conglomerate)	Walkunji conglomerates (Kartikere conglomerate) and cross-bedded quartzite	
-----Deformed angular unconformity-----				
Peninsular gneiss with trondjemite-granodiorite plutons (>3000 Ma)				
-----Intrusive/tectonic contact-----				
Sargur Group (3100–3300 Ma)	Ultramafic-mafic layered complexes, tholeiitic amphibolites, komatiites, BIF Quartzites, pelites, marbles, and calc-silicate rocks			
-----Intrusive/tectonic contact-----				
Gorur Gneiss (3300–3400 Ma)				

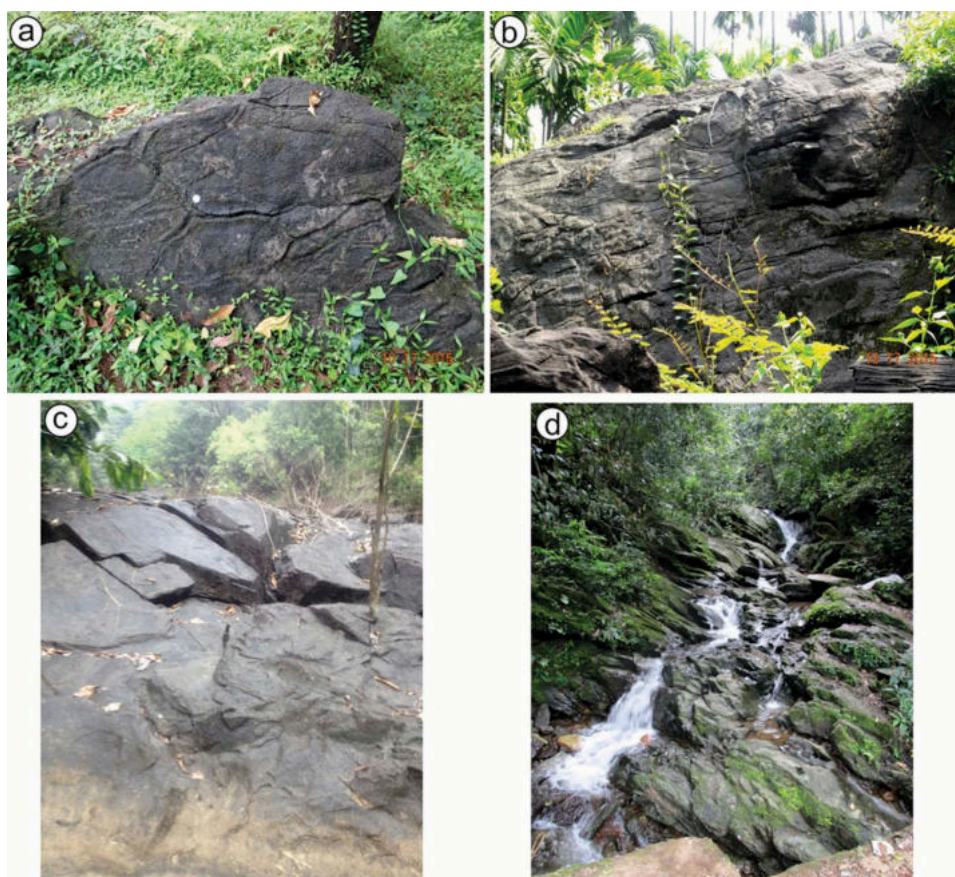


Figure 2. Field photographs: (a) pillow structures in komatiites, (b) massive metavolcanic outcrop in a plantation in Kudremukh region, and (c) metavolcanic exposures along the river channels in Agumbe and Kollur regions.

WGB similar to that of Bababudan belt. The WGB is structurally complex, the upper units being isoclinally folded in large nappes, which have suffered refolding by structures associated with a major N–S sinistral shear belt of presumed Archaean age (Drury and Holt 1980).

As noted earlier, most of the studies carried out so far in the WGB correspond to the metavolcanics, BIFs, and basement gneiss in and around Kudremukh region, though it has been established that the belt extends till Jog Falls in the north through Agumbe, Kodachadri, and Kollur peaks (Figure 1(b)). Hence, metavolcanics and occasionally associated metagabbros sampled throughout the entire stretch of WGB, which were not included in the previous studies by Drury (1981) and Drury *et al.* (1983), forms the focus of this article.

4. Lithology

Ultramafics of Sargur Group, with well-developed pillow structures are exposed prominently in the southern part of the WGB (Figure 2(a)). Pillows are circular to ellipsoidal and have dimensions of ~20–80 cm. They possess distinct rims, radial cracks and vesicles. They are hard,

compact and massive. Metabasalts and occasionally associated metagabbroic sills form part of basic lithologies of Kudremukh and Narsiparvata Formation. They are very well exposed in the river channels, road cuttings and plantations throughout the WGB (Figure 2(b–d)). In fact major part of WGB is covered with metabasalts (Figure 1(b)), but it is highly inaccessible due to thick vegetation cover. This makes sufficient sampling in the belt a bit too difficult. The metabasalts exhibit banding and well developed foliations. Development of asbestos along the joint and shear planes of metabasalts is a common feature observed along the entire stretch of Agumbe Ghat section. Metagabbros occurring as sills within metabasalts are very rare and at many places show intense weathering.

Ultramafics of Sargur Group show ubiquitous concordance with the fabric of the surrounding Peninsular Gneiss, which has a regional anticlinal fold plunging southeast. The Dharwar Supergroup of rocks in the Kudremukh region are deformed in a regional syncline overfolded to the east, marked by conspicuous WNW foliation and 20–50° easterly dips. Minor folds in several areas in the western limb of the major fold indicate

shallow northerly plunges (Swami Nath and Ramakrishnan 1981). Lineations of amygdules in the metabasalts are subparallel to the fold axis showing northerly plunge. The entire litho package studied is metamorphosed to greenschist to lower amphibolite facies.

5. Sampling and analytical techniques

Relatively fresh homogeneous representative samples were collected from road cuttings, streams and outcrops. Weathered and jointed surfaces with quartz/calcite veins were avoided. Twenty-seven metavolcanic and 16 metagabbro samples were collected covering the entire greenstone belt. After petrographic screening for altered mineralogy, samples were analysed for major, trace and rare earth element concentrations at *Institut Universitaire Europe' en de La Mer (IUEM), Plouzane*. Chips were totally powdered using a boron carbide mortar and pestle. The details of sample preparation are given in Barrat *et al.* (2012). Major oxide concentrations were determined by inductively coupled plasma-atomic emission spectrometry (ICP-AES) using a Horiba Jobin Yvon Ultima 2 spectrometer following the procedure of Cotten *et al.* (1995). The concentrations of trace elements, including REEs were determined by

sector field ICPMS (inductively coupled plasma mass spectrometry) using a Thermo Element 2 spectrometer following the procedures described by Barrat *et al.* (Barrat *et al.* 2007, 2008). BHVO-2 and JB-2 were used as standard reference materials during the analysis for monitoring the accuracy of the data (Supplementary Table 1).

6. Petrography

Samples bordering the schist belt show lower amphibolite facies metamorphism, while the samples from the central parts of the belt show greenschist facies. Ultramafics from the southwestern part of the belt are fine grained varieties with pillowed structures. They have retained the original igneous textures (Figure 3(a, b)) such as spherulitic, variolitic fabric, intergrowth, and occasionally porphyritic. They are affected by post-magmatic hydrothermal alteration and low-grade metamorphism under greenschist to lower amphibolite facies condition with rarely preserved primary igneous mineralogy. They consist of actinolite–tremolite, chlorite, plagioclase, and clinzoisite with minor hornblende and relict amygdules of quartz. Actinolite–tremolite are the altered products of pyroxene. Some of the sections show perfect alignment and lineation of mineral

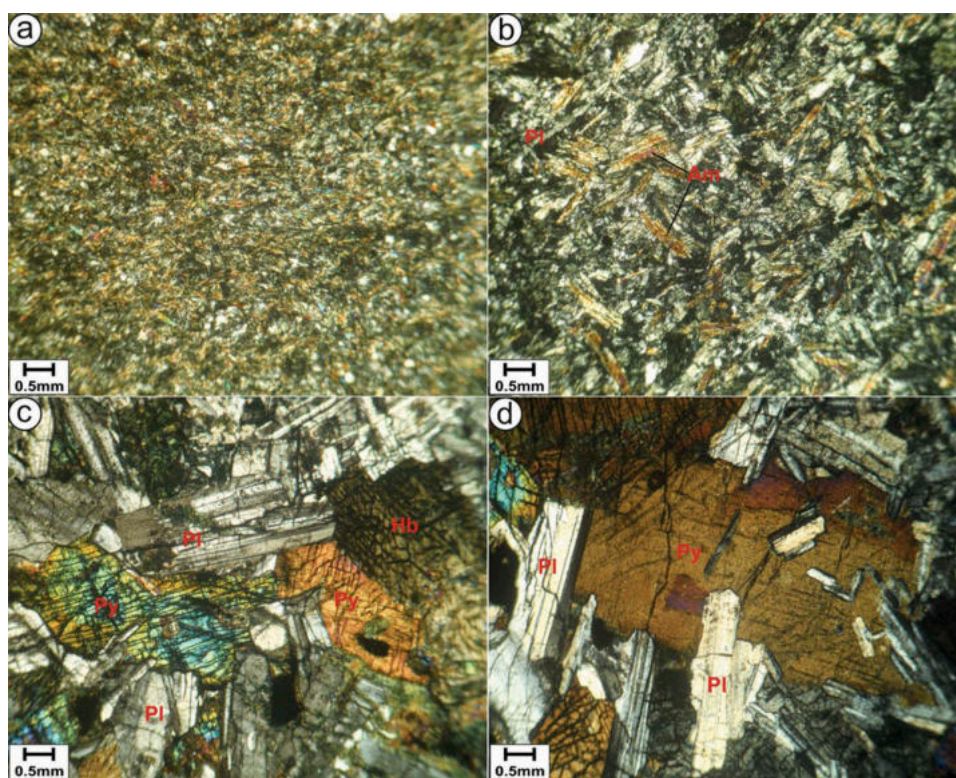


Figure 3. (a) and (b) Photomicrographs of fine and coarse grained metabasalts, respectively. (c) and (d) Photomicrographs of metagabbro showing ophitic to sub-ophitic texture.

exhibiting well developed schistosity. Medium-to-fine-grained metabasalts are massive and schistose, essentially composed of hornblende and plagioclase with relict amygdules of quartz. Hornblende occurs as stumpy or fibrous aggregates and shows local alteration to chlorite. Plagioclase occupies the intergranular spaces between the hornblende grains. Biotite and quartz are subordinate. Metagabbro is a medium-to-coarse-grained, occurring as sills in association with metabasalts. Microscopic study reveals ophitic to sub-ophitic texture, in which the plates of plagioclase feldspars are embedded within the irregular pyroxenes (Figure 3(c,d)). Plagioclase dominates in some of the sections followed by pyroxenes and occasional amphiboles. Bluish-green magnesio-hornblende is rare. The intensely fractured plagioclase is dominantly relict igneous plagioclase generally found in the more altered varieties. Clinzoisite and epidote are secondary after feldspars, while sphene occurs as accessory.

7. Geochemical results

Major and trace element compositions together with element ratios of ultramafics, metabasalts, and associated metagabbros from WGB are given in Table 2.

7.1. Ultramafic unit – komatiites

Based on the definition of komatiites of Arndt and Nesbitt (1982), ultramafic rocks of WGB are classified as komatiites. This is consistent with $\text{Al}_2\text{O}_3\text{--Fe}_2\text{O}_3 + \text{TiO}_2\text{--MgO}$ (Figure 4(a); Jensen 1976) and $\text{CaO--MgO--Al}_2\text{O}_3$ (Figure 4(b); Viljoen *et al.* 1982) ternary plots. However, the characteristic spinifex texture of komatiites is not seen in the studied samples. The obliteration of spinifex texture may be due to deformation and metamorphism, as is the case in many Archaean greenstone belts (Jayananda *et al.* 2008; Ugarkar *et al.* 2014). They have lower $\text{Al}_2\text{O}_3/\text{TiO}_2$ and $\text{CaO}/\text{Al}_2\text{O}_3$ ratios (11 and 0.83–0.91, respectively), and $(\text{Gd}/\text{Yb})_N > 1$ (av. 1.30), by virtue of which they are considered as Al-depleted (Barberton-type) komatiites (Arndt 1994; Sproule *et al.* 2002; Arndt *et al.* 2008). Komatiites of WGB are less siliceous, more magnesian, and Cr (1938–1971 ppm) and Ni (1835–1846 ppm) rich. SiO_2 , Al_2O_3 , Fe_2O_3 , TiO_2 , and P_2O_5 exhibit strong negative correlation with MgO, while Ni is strongly positively correlated with MgO (Figure 5). Ni, TiO_2 , and P_2O_5 of komatiites plot on the olivine control line, while SiO_2 and Al_2O_3 plot below and Fe_2O_3 plot above the olivine control line (Figure 5). They have total REE of 8.05–8.35 ppm and LREE concentrations are three times chondrite. They possess LREE-depleted $[(\text{La}/\text{Sm})_N = 0.60\text{--}0.75]$ and slightly fractionated HREE $[(\text{Gd}/\text{Yb})_N = 1.27\text{--}1.28]$ patterns with

significant negative Eu anomalies (Figure 6(a)). Primitive mantle-normalized patterns of komatiites are near flat from Th–Yb, with slight negative anomalies at Na, Ta, and Zr (Figure 6(b)).

7.2. Mafic unit – high Mg-basalts and basalts

Mafic rocks of WGB are classified as high-Mg basalts (HMBs) and basalts based on their MgO and transitional element (Cr and Ni) concentration. Low siliceous ($\text{SiO}_2 = 46.92\text{--}50.53$ wt%) and high-magnesian ($\text{MgO} = 16.5\text{--}20$ wt%) mafic rocks are classified as HMB, while high siliceous ($\text{SiO}_2 = 48.80\text{--}54.88$ wt%) and low magnesian ($\text{MgO} = 3.4\text{--}8.56$ wt%) mafic rocks are classified as basalts (Table 2). Majority of the basalts of WGB plot in the field of basaltic andesite in total alkali-silica (TAS) diagram (Figure 7(a)) of Le Bas *et al.* (1986), while most of them occupy sub-alkaline basalts field in Nb/Y versus Zr/TiO₂ binary diagram (Figure 7(b); Winchester and Floyd 1977). Sample CJ-21 makes an exception with SiO_2 57.75 wt% and plots in the field of andesite in TAS binary diagram (Figure 7(a)). For the sake of convenience, henceforth the studied basalts and basaltic andesites will be addressed as basalts. The HMB and basalts show sub-alkaline tholeiitic affinity on the AFM ternary plot (Figure 4(c)) of Irvine and Baragar (1971). The HMB show Mg-enrichment, while basalts show Fe-enrichment (Figure 4(c)). Mg# of HMB varies from 57 to 62, while that of basalts from 22 to 44. Plots of MgO versus major oxides and Ni show strong negative correlation with SiO_2 , TiO_2 , Fe_2O_3 , Al_2O_3 , and P_2O_5 , and strong positive correlation with Ni (Figure 5). Most basalts plot on or very close to the olivine control line for SiO_2 , TiO_2 , Al_2O_3 , and Ni, while for Fe_2O_3 and P_2O_5 , they plot below and above the olivine control line, respectively, (Figure 5). Similarly, Ni of HMB plot on the olivine control line, however, SiO_2 and Fe_2O_3 plots very close to, TiO_2 and P_2O_5 plots above, and Al_2O_3 plots below the olivine control line.

HMBs have lower concentrations of total REE (42.1–9.81 ppm) than the basalts (41.65–158.28 ppm) of WGB. LREE concentrations of HMB are 19–38 times chondrite. Chondrite-normalized REE patterns (Figure 6(c)) display flat to slightly enriched LREE and slight to moderately fractionated HREE, with $(\text{La}/\text{Sm})_N = 1.20\text{--}1.76$, $(\text{Gd}/\text{Yb})_N = 1.68\text{--}2.37$, and $(\text{La}/\text{Yb})_N = 2.42\text{--}5.70$ (Table 2). Contrarily, LREE concentrations of basalts are 20–88 times chondrite, with slight to moderately enriched LREE and slightly fractionated HREE patterns on the chondrite-normalized REE plot (Figure 6(e)). They are characterized by $(\text{La}/\text{Sm})_N = 1.03\text{--}4.27$, $(\text{Gd}/\text{Yb})_N = 1.28\text{--}2.06$, and $(\text{La}/\text{Yb})_N = 1.42\text{--}11.54$ (Table 2). Except a sample (CJ-33), all the HMB are characterized

Table 2. Major, trace, and rare earth element (REE) analyses of metavolcanics and metagabbros of Western Ghat belt (WGB).

Samples	CJ26 K	CJ27 K	CJ-9 HMB	CJ22 HMB	CJ37 HMB	CJ38 HMB	CJ33 HMB	CJ34 HMB	CJ-1 B	CJ14 B	CJ-5 B
SiO ₂	42.44	42.21	48.83	50.53	46.92	47.33	49.37	48.87	52.01	52.08	53.61
TiO ₂	0.3	0.3	0.82	0.73	0.99	0.99	1.08	0.87	1.05	0.94	0.91
Al ₂ O ₃	3.3	3.16	5.51	5	6.4	5.98	6.29	6.42	12.94	12.07	13.87
Fe ₂ O ₃	13.17	13.65	13.06	12.86	14.55	14.51	13.85	13.87	14.66	11.86	12.41
MnO	0.15	0.16	0.2	0.19	0.19	0.19	0.31	0.2	0.19	0.16	0.17
MgO	30.54	28.88	18.46	18.76	20.02	20	16.5	18.87	5.03	8.56	6.07
CaO	2.99	2.61	8.51	9.32	5.46	5.65	9.01	8.33	8.77	9.22	8.4
Na ₂ O	0.12	0.16	0.17	0.15	0.09	0.1	0.44	0.23	3.19	2.96	2.59
K ₂ O	0.01	0.01	0.03	0.02	0.01	0.01	0.03	0.01	0.19	0.11	0.25
P ₂ O ₅	0.05	0.04	0.09	0.1	0.11	0.11	0.13	0.11	0.12	0.11	0.11
LOI	8.04	7.76	3.01	2.74	3.66	3.52	1.82	2.91	1.08	2.04	1.27
Total	101.1	98.94	98.69	100.41	98.42	98.4	98.83	100.7	99.22	100.1	99.66
Cr	1971	1938	1114	887	2000	1873	1817	1569	60	848	180
Co	126	115	82	89	111	108	84	96	64	69	57
Ni	1835	1846	867	733	1336	1291	939	1078	97	298	154
Rb	0.2	0.43	0.47	0.59	0.28	0.25	0.09	0.09	0.55	2.34	2.76
Sr	20.02	37.4	6.31	6.85	28.71	28.99	12.54	5.18	93.34	316.11	129.81
Cs	0.11	0.33	0.08	0.11	0.38	0.37			0.02	0.02	0.05
Ba	0.21	0.17	3.1	1.57	1.65	1.83	0.7	2.28	23.47	46.85	126.29
Ti	1806	1820	4936	4388	5962	5926	6467	5244	6291	5653	5467
Sc	17.24	16.69	17.89	18.45	24.43	24.5	25.74	24.17	31.75	33.24	30.94
V	112	121	149	158	191	190	214	180	297	246	251
Ta	0.05	0.05	0.32	0.34	0.46	0.44	0.37	0.3	0.2	0.19	0.3
Nb	0.85	1.02	4.69	4.63	8.03	7.56	6.12	4.47	3	2.95	4.27
Zr	7.89	8.32	73.4	77.43	91.71	85.88	84.43	84.05	48.33	36.68	49.86
Hf	0.29	0.27	2.07	2.14	2.58	2.41	2.4	2.39	1.36	1.15	1.45
Th	0.15	0.15	1.32	1.15	1.08	1.05	0.71	1.43	1.08	0.82	2.19
U	0.11	0.2	0.32	0.33	0.27	0.26	0.2	0.33	0.29	0.17	0.47
Y	5.15	5.44	17.74	21.07	16.01	16.35	21.67	16.57	23.01	19.16	33.08
La	0.57	0.7	7.74	5.66	10.18	9.92	5.84	9.33	8.66	11.81	16.18
Ce	1.64	1.8	15.07	10.39	24.67	23.77	12.99	22.51	19.55	17.06	26.29
Pr	0.28	0.3	2.36	1.65	3.58	3.46	2.05	3.21	2.69	3.1	4.75
Nd	1.58	1.6	10.53	8.58	15.87	15.79	11.02	14.76	12.23	13.58	19.86
Sm	0.59	0.58	2.8	2.75	3.61	3.75	3.05	3.43	3.31	3.48	5.24
Eu	0.11	0.12	0.71	0.68	0.9	0.93	1.33	0.55	1.24	1.25	1.54
Gd	0.83	0.84	3.2	3.54	3.66	3.93	3.6	3.29	4.05	3.61	5.8
Tb	0.14	0.14	0.53	0.57	0.55	0.59	0.66	0.51	0.66	0.58	0.99
Dy	0.93	0.9	3.2	3.6	3.15	3.22	4.09	3.1	3.97	3.3	6.11
Ho	0.2	0.2	0.64	0.73	0.6	0.63	0.78	0.61	0.81	0.64	1.21
Er	0.56	0.57	1.71	2.04	1.57	1.64	2.18	1.62	2.2	1.57	3.34
Yb	0.53	0.53	1.54	1.68	1.28	1.34	1.68	1.42	1.76	1.42	2.99
Lu	0.08	0.08	0.21	0.23	0.18	0.19	0.22	0.2	0.24	0.18	0.42
Cu	40	67	23	2	207	228	19	55	109	149	109
Pb	0.96	1.39	1.13	1.26	1.67	1.86	1.16	0.93	2.79	2.61	5.35
Zn	58	83	134	131	94	89	237	88	107	95	104
Ga	6.03	6.07	8.78	9.03	10.96	10.35	11.12	10.73	18.42	15.83	19.49
Be	0.19	0.42	0.65	0.69	0.68	0.69	1.35	0.56	0.6	0.56	0.8

Samples	CJ-6 B	CJ7 B	CJ21 B	CJ43 B	CJ-8 B	CJ35 B	CJ36 B	CJ41 B	CJ-12 B	CJ28 B
SiO ₂	53.31	54.19	57.75	53.22	54.33	52.28	52.12	53.61	52.99	54.88
TiO ₂	0.9	0.84	1.18	0.92	0.83	0.94	0.96	0.85	0.8	0.75
Al ₂ O ₃	13.87	13.47	12.67	14.04	13.99	12.06	12.22	14.51	14.32	14.84
Fe ₂ O ₃	12.32	11.49	13.14	12.34	11.88	12.29	12.21	11.75	11.76	10.8
MnO	0.17	0.17	0.19	0.17	0.18	0.16	0.16	0.17	0.17	0.16
MgO	6.09	6.12	3.4	5.93	6.27	8.3	8.39	6.13	6.27	5.93
CaO	8.91	10.42	7.79	8.42	9.79	10.62	10.32	9.93	9.59	8.92
Na ₂ O	2.57	2.73	2.68	2.62	2.22	2.34	2.53	2.31	3.24	2.59
K ₂ O	0.23	0.26	0.24	0.23	0.16	0.13	0.12	0.14	0.2	0.19
P ₂ O ₅	0.11	0.12	0.16	0.13	0.13	0.11	0.11	0.14	0.13	0.1
LOI	1.34	0.68	0.79	1.13	0.65	0.62	0.6	0.62	0.8	1.06
Total	99.83	100.5	99.99	99.14	100.43	99.84	99.75	100.16	100.27	100.22
Cr	179	211	30	178	147	775	774	143	224	119
Co	55	50	56	56	49	70	71	50	47	50
Ni	151	150	70	151	106	290	291	108	123	138
Rb	2	1.9	2.22	2.72	0.69	0.69	0.63	0.7	0.94	1.03
Sr	128.01	159.26	105.38	125.47	83.78	277.29	283.18	94.85	268.9	102.49
Cs	0.04	0.02			0				0.02	
Ba	37.41	34.26	47.97	42.34	13.09	30.47	35.37	10.46	137.28	59.31
Ti	5420	5042	7076	5520	5003	5629	5731	5110	4817	4468
Sc	30.45	30.82	30.79	31.58	33.69	31.78	32.03	35.89	33.95	28.96

(Continued)

Table2. (Continued).

Samples	CJ-6 B	CJ7 B	CJ21 B	CJ43 B	CJ-8 B	CJ35 B	CJ36 B	CJ41 B	CJ-12 B	CJ28 B
V	253	215	293	259	230	254	252	244	226	226
Ta	0.3	0.41	0.48	0.32	0.33	0.2	0.22	0.35	0.26	0.39
Nb	4.21	5.39	6.17	4.34	4.3	3.24	3.13	4.65	3.58	4.94
Zr	46.87	48.92	116.07	43.23	43.6	19.88	32.22	44.37	36.39	50.95
Hf	1.39	1.38	3.28	1.37	1.25	0.68	1.07	1.35	1.05	1.62
Th	2.12	3.11	3.44	2.27	2.55	0.94	0.99	2.77	2.02	2.96
U	0.45	1	1.09	0.48	0.78	0.22	0.19	0.92	0.58	0.97
Y	34.77	25.68	45.72	32.2	30.62	14.91	15.32	35.04	26.89	24.89
La	35.62	15.23	35.52	49.39	12.67	5.34	4.95	15.39	10.13	12.19
Ce	27.5	26.6	64.95	27.99	24.54	13.32	12.33	27.99	21.46	27.1
Pr	7.79	4.12	8.21	9.8	3.69	1.95	1.81	4.12	2.75	3.3
Nd	31.28	16.25	34.25	40.3	15.45	9.16	8.67	17.29	11.78	13.49
Sm	6.33	3.78	7.6	7.23	3.97	2.63	2.64	4.29	2.98	3.38
Eu	1.84	1.06	2.06	1.87	1.09	0.99	0.97	1.18	1.02	1.2
Gd	6.34	4.01	8.4	6.54	4.58	2.91	3.14	5.28	3.57	3.78
Tb	1.01	0.68	1.26	1.03	0.78	0.46	0.51	0.88	0.64	0.67
Dy	6.01	4.39	7.46	6.08	5	2.82	3.02	5.48	4.16	4.33
Ho	1.18	0.91	1.48	1.24	1.07	0.57	0.58	1.18	0.91	0.93
Er	3.21	2.55	4.11	3.33	3.03	1.42	1.58	3.27	2.66	2.54
Yb	2.79	2.35	3.52	3.07	2.83	1.25	1.27	2.98	2.5	2.48
Lu	0.39	0.32	0.47	0.42	0.39	0.17	0.18	0.43	0.34	0.32
Cu	108	63	255	105	111	50	56	97	82	89
Pb	5.29	9.29	6.62	5.76	8.33	3.56	3.74	9.42	3.6	5.47
Zn	99	88	102	99	100	90	89	96	93	82
Ga	19.36	16.76	18.25	19.47	15.06	18.5	17.22	16.45	16.35	16.97
Be	0.83	0.89	0.91	0.74	0.78	0.56	0.56	0.75	0.63	0.8
Samples	CJ29 B	CJ30 B	CJ-2 Bo	CJ-3 Bo	CJ20 Bo	CJ40 Bo	CJ-10 Ga	CJ-11 Ga	CJ13 Ga	CJ15 Ga
SiO2	53.4	48.8	49.22	48.53	50.32	48.85	50.17	51.31	49.61	50.05
TiO2	1.56	2.11	0.39	0.35	0.35	0.39	1.13	0.79	1.58	1.11
Al2O3	12.89	15.13	11.41	11.04	10.91	11.76	15.04	14.48	13.55	15.3
Fe2O3	13.33	15.03	10.53	11.21	11.04	11.02	14.02	12.35	15.76	13.33
MnO	0.18	0.18	0.16	0.18	0.18	0.17	0.2	0.18	0.21	0.19
MgO	5.6	4.13	13.88	14.73	14.16	13.73	6.55	6.07	5.58	5.93
CaO	8.95	9.91	8.62	8.48	8.4	8.16	10.15	11.44	9.76	9.85
Na2O	2.94	3.23	2.22	1.99	2.08	2.11	2.27	1.93	2.26	2.3
K2O	0.41	0.44	0.05	0.04	0.03	0.02	0.53	0.16	0.85	0.55
P2O5	0.15	0.18	0.05	0.06	0.06	0.06	0.16	0.11	0.21	0.16
LOI	0.84	0.76	3.24	3.63	3.45	3.45	0.22	0.79	1.32	0.46
Total	100.25	99.91	99.78	100.22	100.98	99.73	100.44	99.62	100.7	99.23
Cr	278	28	1557	1831	1694	1586	186	92	141	190
Co	41	38	62	67	75	73	55	50	58	53
Ni	127	40	464	576	556	474	139	104	94	124
Rb	12.78	12.21	0.45	0.28	0.34	0.47	17.04	1.44	30.58	18.2
Sr	109.59	139.83	74.74	53.75	53.16	75.7	137.88	54.54	177.45	144.8
Cs	0.24	0.31	0.08	0.07	0.07	0.11	0.61	0.01	1.32	0.7
Ba	21.71	23.62	6.58	3.55	3.65	4.51	118.23	19.22	246.77	130.03
Ti	9327	12620	2333	2100	2109	2358	6758	4717	9452	6651
Sc	32.06	33.61	33.66	31.02	34.53	38.76	34.66	32.58	42.64	33.58
V	560	723	178	163	179	206	241	233	295	228
Ta	0.27	0.34	0.12	0.11	0.12	0.14	0.3	0.29	0.48	0.33
Nb	3.93	5	1.6	1.45	1.63	1.81	4.36	4	7.1	4.49
Zr	20.14	20.42	12.2	12.26	16.08	10.94	115.94	35.99	111.87	115.12
Hf	1.04	1.18	0.42	0.4	0.51	0.4	3.11	1.13	3.07	3.41
Th	0.65	0.72	0.96	0.92	0.87	1.1	1.7	2.18	4.25	1.79
U	0.27	0.38	0.31	0.29	0.3	0.36	0.46	0.63	1.22	0.5
Y	34.49	51.72	17.08	15.1	15.91	17.9	30.16	24.43	37.69	31.7
La	6.03	10.93	5.18	3.52	3.63	5.19	10.31	12.55	14.25	10.82
Ce	15.11	25.21	10.74	7.74	8.26	11	22.87	25.46	28.95	24.03
Pr	2.3	3.6	1.35	1.02	1.07	1.44	3.08	3.16	3.71	3.3
Nd	11.4	17.43	5.59	4.39	4.6	5.86	14.01	13.07	16.86	15.22
Sm	3.67	5.18	1.39	1.18	1.23	1.49	3.79	3.11	4.38	4.11
Eu	1.58	2.4	0.51	0.39	0.37	0.5	1.17	0.92	1.52	1.28
Gd	4.96	6.99	1.89	1.66	1.76	2.07	4.6	3.56	5.36	4.67
Tb	0.87	1.25	0.36	0.32	0.35	0.4	0.78	0.61	0.89	0.82
Dy	5.51	8.11	2.5	2.29	2.5	2.8	4.93	3.96	5.63	5.07
Ho	1.19	1.72	0.59	0.54	0.56	0.65	1.05	0.85	1.22	1.1
Er	3.29	4.76	1.78	1.65	1.72	1.99	2.93	2.41	3.55	3.01

(Continued)

Table2. (Continued).

Samples	CJ-6 B	CJ7 B	CJ21 B	CJ43 B	CJ-8 B	CJ35 B	CJ36 B	CJ41 B	CJ-12 B	CJ28 B
Yb	3.05	4.42	1.59	1.51	1.58	1.74	2.69	2.2	3.54	2.94
Lu	0.44	0.62	0.22	0.21	0.22	0.24	0.39	0.3	0.5	0.44
Cu	90	181	40	31	25	41	177	75	157	171
Pb	1.34	1.83	2.25	1.45	1.39	2.06	3.38	4.22	5.44	3.95
Zn	102	104	66	66	69	71	112	92	109	97
Ga	22.78	30.23	10.44	9.45	9.48	11.62	19.34	16.95	18.82	19.56
Be	0.86	0.92	0.28	0.25	0.26	0.27	0.66	0.75	0.84	0.66
Samples	CJ16 Ga	CJ17 Ga	CJ18 Ga	CJ19 Ga	CJ23 Ga	CJ24 Ga	CJ25 Ga	CJ31 Ga	CJ32 Ga	CJ39 Ga
SiO2	50.47	50.63	50.55	50.12	52.26	52.38	52.43	49.53	48.7	54.21
TiO2	1.12	1.1	1.12	1.16	0.62	0.62	0.63	1.81	1.98	0.96
Al2O3	15.19	15.72	14.98	14.9	14.92	11.08	11.43	16.45	16.37	14.61
Fe2O3	13.89	13.51	13.95	13.92	11.85	11.63	11.47	16.15	16.98	11.99
MnO	0.2	0.19	0.2	0.2	0.18	0.19	0.18	0.2	0.21	0.15
MgO	6.45	5.99	6.44	6.47	6.35	10.28	10.06	3.61	3.59	5.8
CaO	10.21	10.15	10.29	10.28	11.13	10.08	10.01	9.53	9.27	8.43
Na2O	2.27	2.38	2.28	2.23	2.07	1.63	1.71	2.74	2.7	3.34
K2O	0.52	0.55	0.48	0.49	0.3	0.41	0.41	0.74	0.78	0.1
P2O5	0.15	0.17	0.16	0.15	0.08	0.09	0.09	0.24	0.25	0.14
LOI	0.39	0.45	0.38	0.45	0.71	1.52	1.56	-0.05	-0.12	0.43
Total	100.87	100.84	100.82	100.37	100.48	99.9	99.97	100.95	100.71	100.16
Cr	213	178	212	220	122	860	812	35	39	16
Co	56	52	56	56	52	63	60	49	54	57
Ni	136	124	138	137	103	287	280	68	75	129
Rb	18.31	18.76	16.94	16.69	5.86	21.97	22.8	25.14	25.94	0.52
Sr	141.78	147.86	145.96	139.32	94.81	129.14	134.79	154.33	157.08	248.82
Cs	0.72	0.79	0.67	0.67	0.4	1.08	1.14	1.36	1.42	
Ba	122.73	130.68	116.76	116.14	43.9	63.4	65.57	176.8	182.79	15.3
Ti	6726	6613	6689	6964	3688	3730	3778	10865	11875	5734
Sc	35.71	33.02	35.69	34.8	40.52	35.16	33.98	28.27	27.73	32.86
V	240	221	242	242	219	226	213	227	292	247
Ta	0.31	0.34	0.33	0.32	0.3	0.2	0.21	0.5	0.47	0.65
Nb	4.43	4.82	4.44	4.42	3.87	2.74	2.9	7.08	6.84	8.1
Zr	116.74	126.17	126.11	116.69	59.65	45.18	54.91	167.44	164.01	134.94
Hf	3.36	3.56	3.44	3.36	1.79	1.37	1.66	4.69	4.59	3.79
Th	1.79	1.88	1.91	1.73	2.64	1.51	1.55	2.68	2.56	5.67
U	0.55	0.55	0.49	0.46	0.66	0.42	0.45	0.73	0.71	2.18
Y	32	33.22	32.81	32.21	27.8	19.32	19.63	45.22	43.63	33.01
La	10.58	11.38	10.4	10.26	10.23	7.94	8.13	16.16	16.69	21.22
Ce	23.62	25.41	23.93	23.95	20.79	17.01	17.19	36.97	37.1	43.63
Pr	3.38	3.69	3.43	3.22	2.59	2.18	2.18	4.72	4.77	5.33
Nd	14.97	15.93	15.13	14.21	10.64	9.24	9.55	22.12	21.72	20.94
Sm	4.02	4.18	3.96	3.93	2.63	2.32	2.42	5.74	5.59	4.89
Eu	1.27	1.35	1.32	1.26	0.79	0.79	0.82	1.77	1.75	1.32
Gd	4.91	4.83	4.67	4.86	3.48	2.96	3.02	6.95	6.6	5.29
Tb	0.83	0.85	0.83	0.84	0.63	0.52	0.51	1.16	1.1	0.89
Dy	5.17	5.64	5.36	5.25	4.47	3.32	3.21	6.96	6.79	5.46
Ho	1.1	1.15	1.15	1.09	1.01	0.74	0.73	1.48	1.39	1.2
Er	3.16	3.27	3.21	3.11	2.92	1.99	2	4.25	4.17	3.28
Yb	3.04	3.08	3.05	2.8	2.8	1.83	1.88	3.99	3.76	3.12
Lu	0.43	0.46	0.45	0.39	0.43	0.26	0.28	0.57	0.56	0.44
Cu	168	166	181	183	60	119	164	261	296	120
Pb	3.88	4.26	3.95	4.02	3.8	6.32	6.6	5.55	5.77	9.68
Zn	100	95	101	97	79	77	73	124	139	92
Ga	19.92	19.57	19.33	18.95	16.43	13.78	13.64	23.35	23.76	19.48
Be	0.63	0.67	0.66	0.61	0.53	0.45	0.47	0.98	0.94	1.1
Samples	CJ42 Ga									CJ-4 Ga
SiO2	50.13									56.36
TiO2	1.06									1.19
Al2O3	15.05									13.04
Fe2O3	13.46									14.35
MnO	0.2									0.19
MgO	6.24									3.62
CaO	10.08									7.71
Na2O	2.25									2.63
K2O	0.52									0.28
P2O5	0.16									0.16

(Continued)

Table 2. (Continued).

Samples	CJ42 Ga	CJ-4 Ga
LOI	0.36	0.37
Total	99.49	99.91
Cr	190	22
Co	56	55
Ni	135	73
Rb	18.7	2.43
Sr	140.64	93.09
Cs	0.91	0.01
Ba	115.79	46.55
Ti	6326	7131
Sc	35.06	31.43
V	233	303
Ta	0.31	0.45
Nb	4.32	6.08
Zr	107.98	84.99
Hf	3.1	2.34
Th	1.68	3.23
U	0.43	0.94
Y	31.4	35.86
La	10.08	17.18
Ce	22.15	47.14
Pr	3.07	5.02
Nd	13.92	20.21
Sm	3.86	5.16
Eu	1.28	1.46
Gd	5.01	5.56
Tb	0.83	0.97
Dy	5.11	6.06
Ho	1.08	1.26
Er	3.03	3.54
Yb	2.85	3.24
Lu	0.41	0.44
Cu	165	145
Pb	4.03	5.57
Zn	106	117
Ga	19.5	18.84
Be	0.6	1.03

K: Komatiites; HMB: high-Mg basalts; B: basalts; Bo: boninites; Ga: metagabbros.

by moderate to weak negative Eu anomalies ($\text{Eu}/\text{Eu}^* = 0.49\text{--}0.75$), while basalts are characterized by slightly positive to moderately negative Eu anomalies ($\text{Eu}/\text{Eu}^* = 0.76\text{--}1.22$). Few samples of HMB and basalts exhibit negative Ce anomaly (Figure 6(c,e)). Primitive mantle-normalized multi element patterns (Figure 6(d, f)) show relatively more pronounced negative anomalies of Nb, Ta, Zr, and Ti for basalts compared to HMB, suggesting both types are similar to those described for island arc basalts (Sheraton *et al.* 1990; Zhao *et al.* 1995).

7.3. Mafic unit – boninites

SiO_2 of the studied samples varies between 48.53 and 50.32 wt%, with very low TiO_2 (0.35–0.39 wt%) and Nb (1.45 – 1.81 ppm) contents (Table 2). They are characterized by high MgO (13.73–14.73 wt%), Cr (1557–1831 ppm),

and Ni (464–576 ppm) contents, and are distinctive in the conjunction of low abundances of incompatible elements with respect to the studied komatiites of WGB. They also have distinctively lower Nb/Th ratios (1.58–1.87), higher $\text{Al}_2\text{O}_3/\text{TiO}_2$ ratios (29–32) and negatively sloping HREE [$(\text{Gd}/\text{Yb})_N = 0.89\text{--}0.96$] compared to the studied komatiites (Table 2). Collectively, these are compositional characteristics of the boninitic magma series (Brown and Jenner 1989; Crawford *et al.* 1989). Boninites are classified as high- and low-Ca boninites based on the bulk rock $\text{Al}_2\text{O}_3/\text{CaO}$ ratio (Crawford *et al.* 1989). Average $\text{CaO}/\text{Al}_2\text{O}_3$ ratio (0.75) of the studied samples suggests that they are high-Ca boninites. Boninites of WGB represent a separate population in the plots of MgO versus major oxides and Ni (Figure 5). They have lower Ti/Zr, Zr/Y, Hf/Ta, and Hf/Th ratios compared to the komatiites of WGB. Chondrite-normalized REE patterns (Figure 6(g)) show relative enrichment in LREE and HREE with respect to

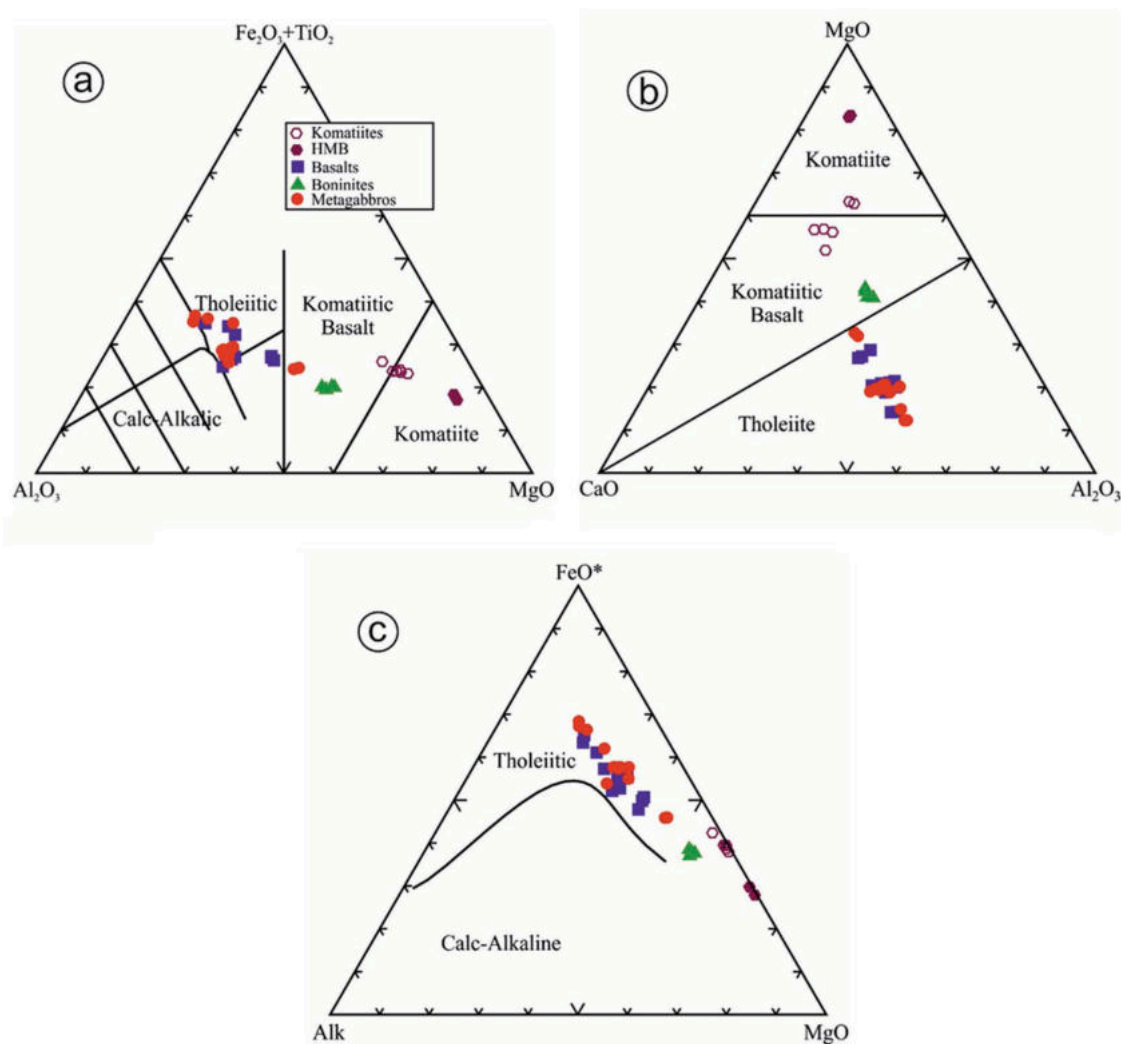


Figure 4. (a) Al_2O_3 – $\text{Fe}_2\text{O}_3 + \text{TiO}_2$ – MgO (Jensen 1976) triangular plot. (b) CaO – MgO – Al_2O_3 triangular plot of Viljoen *et al.* (1982). (c) AFM plot of Irvine and Baragar (1971).

MREE. They are characterized by LREE at about 12–16 times chondrite, with LREE-enriched $[(\text{La}/\text{Sm})_N = 1.84\text{--}2.33]$ and slight to moderately depleted HREE $[(\text{Gd}/\text{Yb})_N = 0.89\text{--}0.96]$ patterns. Primitive mantle-normalized trace element abundances (Figure 6(h)) show negative anomalies at Nb–Ta, Zr–Hf, and Ti.

7.4. Gabbros

There is a strong resemblance in chemistry between the gabbros and basalts of the present study. SiO_2 varies from 48.70 to 54.21 wt% (Table 2) and majority of the samples plot in the field of basalts (gabbro), while few occupy basaltic andesites (gabbrodiorite) field in total alkali-silica (TAS) diagram (Figure 7(a)) of Le Bas *et al.* (1986). While majority of them occupy basaltic andesite (gabbrodiorite) field in Nb/Y versus Zr/TiO₂ binary diagram (Figure 7(b); Winchester and Floyd 1977), one sample falls in the sub-

alkaline basalt (gabbro) field and another on the boundary line separating basaltic andesites (gabbrodiorite) and andesites (diorite). Similar to basalts, gabbros and gabbrodiorites will be henceforth addressed as gabbros for the sake of convenience. Gabbros of WGB show sub-alkaline tholeiitic affinity on AFM diagram, with Fe-enrichment (Figure 4(c)). Plots of MgO versus major oxides and Ni show similar relations as that of basalts (Figure 5).

Gabbros have total REE concentrations of about 51.1–117.23 ppm and are characterized by LREE at about 25–63 times chondrite. Chondrite-normalized REE patterns (Figure 6(i)) display slightly enriched LREE and slightly fractionated HREE, with $(\text{La}/\text{Sm})_N = 1.63\text{--}2.71$, $(\text{Gd}/\text{Yb})_N = 1.22\text{--}2.00$, and $(\text{La}/\text{Yb})_N = 1.42\text{--}4.88$ (Table 2). They are characterized by slight negative Eu anomalies, while Ce anomalies are not observed (except for a sample). Primitive mantle-normalized multi element patterns show pronounced negative Nb, Ta and Ti anomalies (Figure 6(j)). Few samples

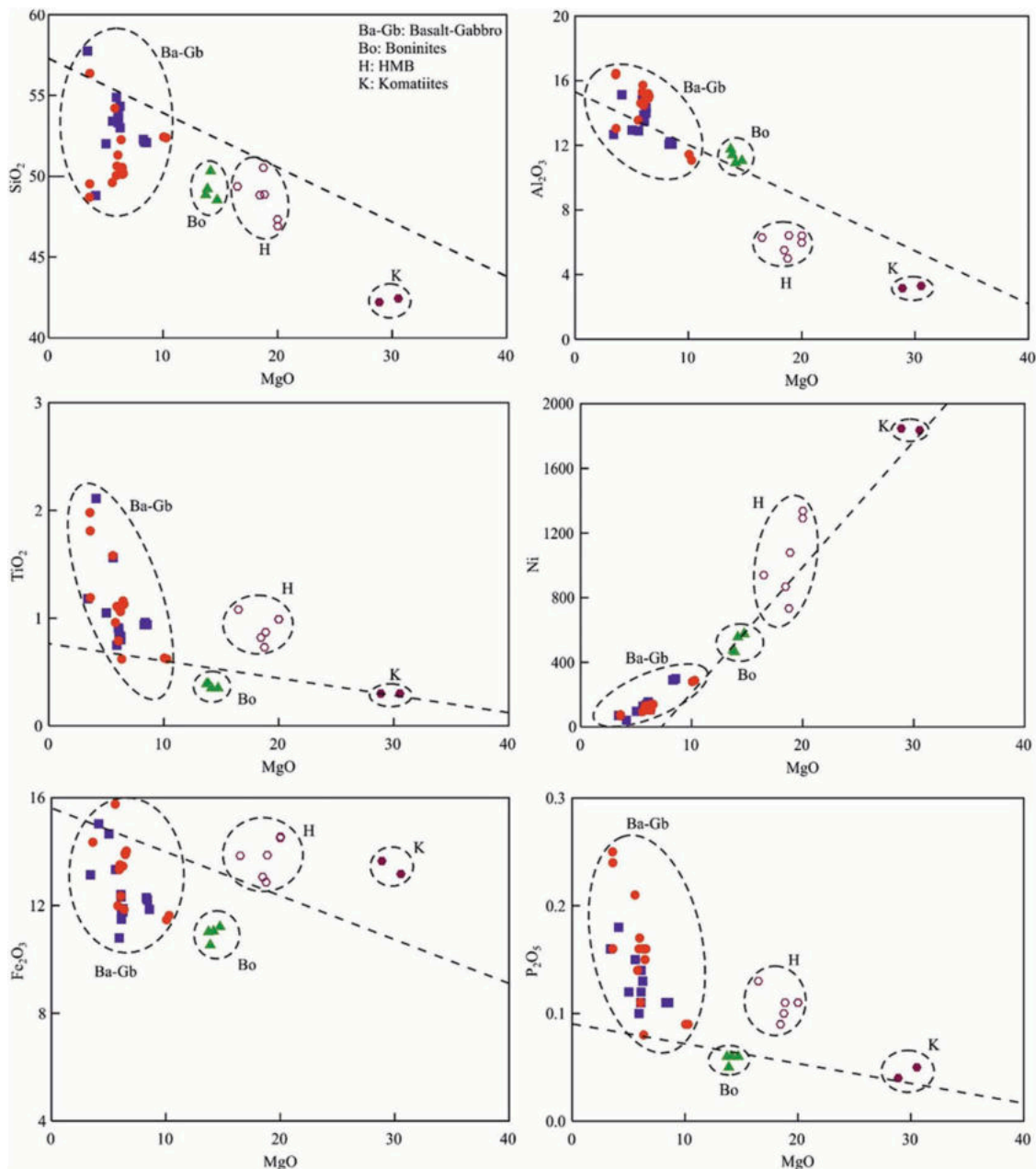


Figure 5. MgO vs. selected major oxides and Ni plot. Dotted line indicates the olivine control line.

are characterized by negative Zr–Hf anomalies, while others display flat patterns. The overall primitive mantle-normalized multi element patterns of the studied gabbros indicate their similarity with those described for island arc basalts (Sheraton *et al.* 1990; Zhao *et al.* 1995).

8. Discussion

8.1. Alteration and element mobility

As the WGB has undergone greenschist to lower amphibolite facies metamorphism, the effects of secondary

element remobilization must be considered. Differential elemental retention during metamorphism by MORB and arc protoliths is useful in distinguishing original protolith trace element composition *versus* modified trace element composition due to varying degrees of mobility of various elements during subduction metamorphism (Ghatak *et al.* 2012). WGB komatiites shows depletion of LREE suggesting that there was no LREE mobility in these rocks during subduction metamorphism. The overall REE patterns of the studied HMB–basalts (and associated gabbros) are essentially

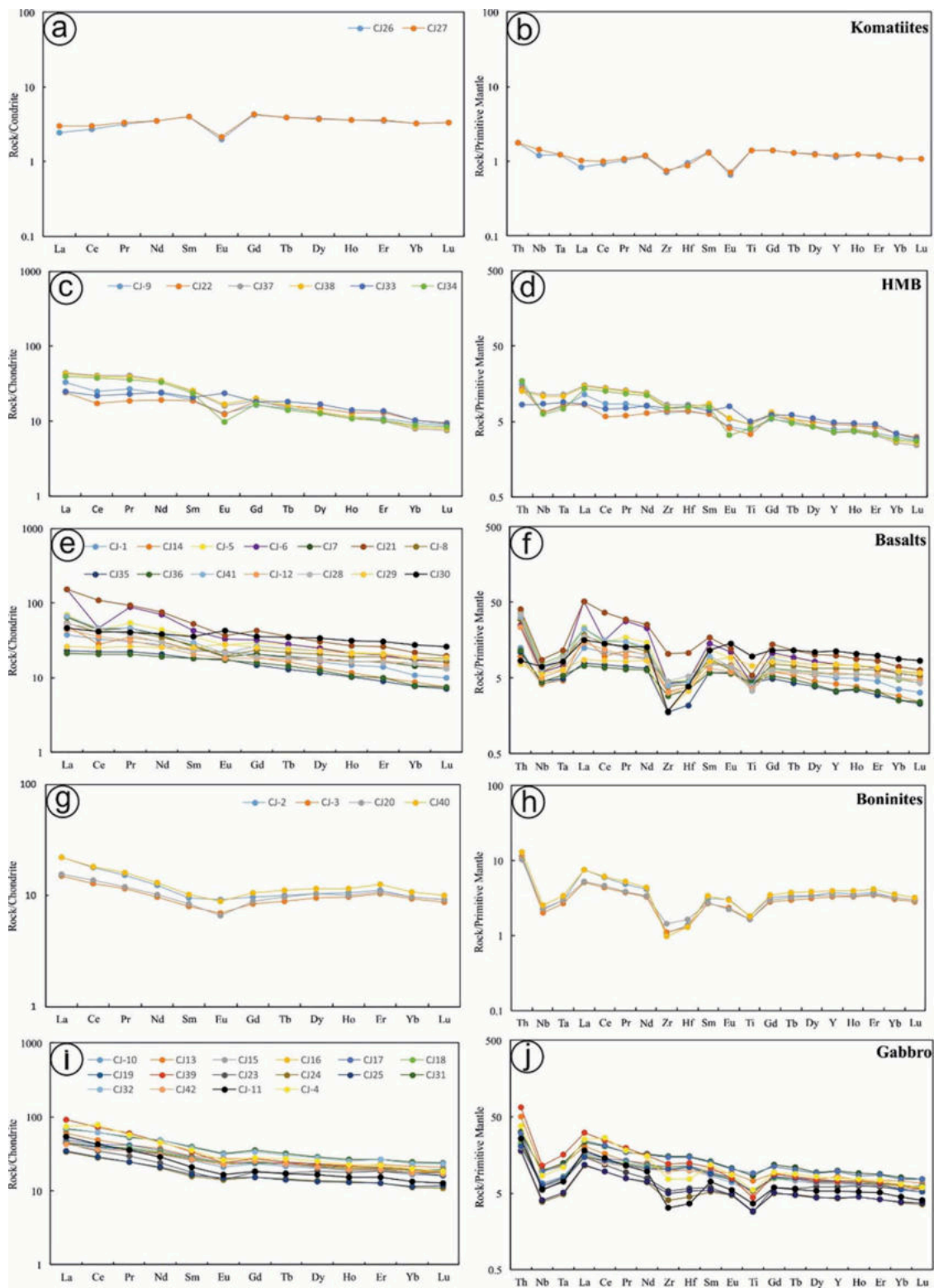


Figure 6. Chondrite-normalized REE and primitive mantle-normalized multi-element plots of komatiites, HMB, basalts, boninites, and metagabbros.

flat similar to nascent arc basalts. They are distinctly different from OIB and enriched MORB (E-MORB) that are characterized by LREE enrichment over HREE (Ghatak *et al.* 2012). Role of pelagic sediments is also

ruled out as the characteristic LREE enrichment of pelagic sediments is not seen in their REE patterns.

The relationship between fluid addition, protolith composition and the presence or absence of a

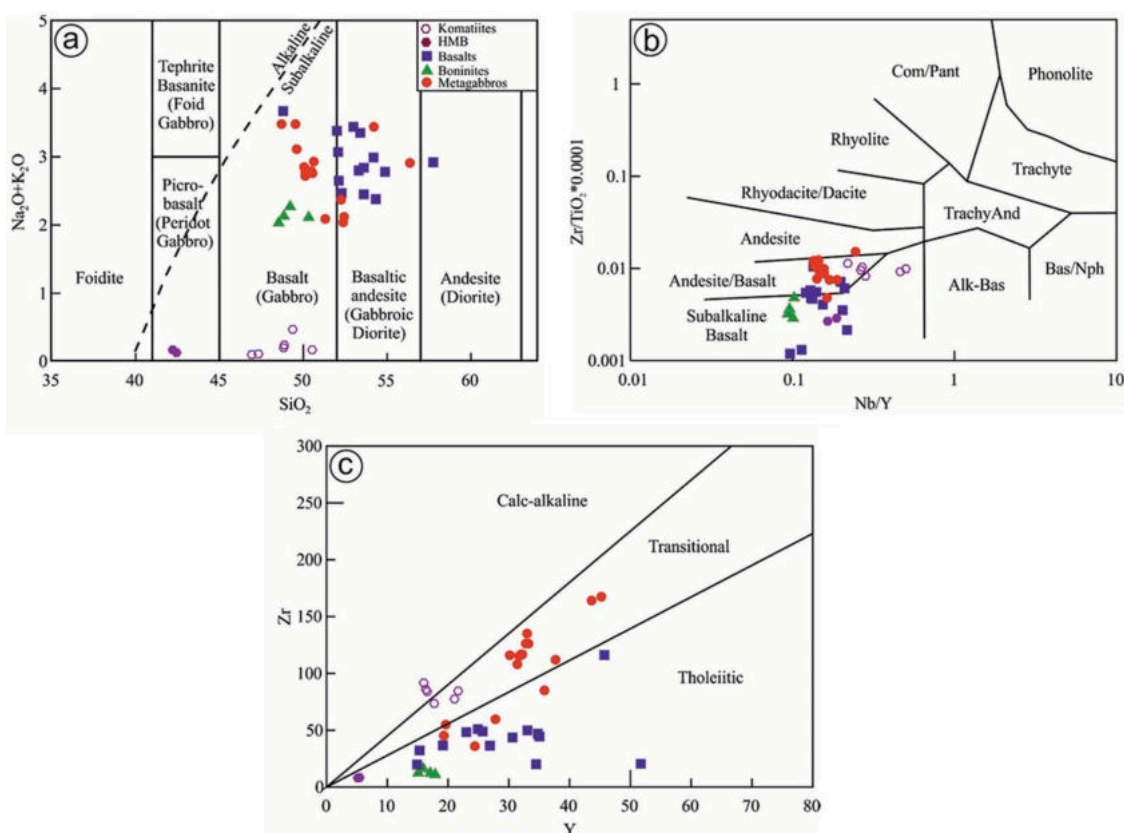


Figure 7. (a) Total-alkali silica diagram of Le Bas *et al.* (1986). (b) Nb/Y vs. $Zr/TiO_2 \cdot 0.0001$ binary plot of Winchester and Floyd (1977). (c) Zr vs. Y plot of Ross and Bedard (2009).

sedimentary component have been effectively evaluated in a plot of Ba/La versus $(La/Sm)_N$ by Ghatak *et al.* (2012). It has been shown that mobility of a fluid rich in Ba increases as the metamorphic grade increases. A plot of Ba/La versus $(La/Sm)_N$ (Figure 8(a)) indicates that there was neither significant fluid addition nor sediment contamination in our studied samples. Further, the chemical index of alteration (CIA) ranging from 39 to 56 and the consistent patterns of selected elements in primitive mantle normalized multielement diagrams (Figure 6) also suggest minimal alteration of the studied rocks (Nesbitt and Young 1982).

Ce/Ce* ratios between <0.9 and >1.1 for the Archaean ultramafic–mafic rock associations indicate LREE mobility, while the ratios between 0.9 and 1.1 suggest negligible LREE mobility (Polat *et al.* 2002). Six basaltic samples and a HMB sample, which indicate LREE mobility with Ce/Ce* ratios falling between <0.9 and >1.1 are exempted from petrogenetic interpretation. Both bulk continental crust and Archaean continental crust estimates show negative Eu anomalies of 0.885 and 0.896, respectively (Rudnick and Fountain 1995; Rudnick and Gao 2014), whereas primary komatiitic lavas cannot have primary Eu anomalies, for there will be neither plagioclase

presence in their sources nor plagioclase involvement in any subsequent crystal–liquid fractionation prior to emplacement. Large scale negative anomaly observed in some of our analysed samples may reflect mobilization of this element by hydrothermal fluids.

The above considerations of relative element mobility are in accordance with the conclusions of previous studies of altered and metamorphosed volcanic rocks, in which Al, Ti, Ni, HFSE, and REE (except Eu, Ce) were regarded as relatively alteration insensitive, and hence, are the representatives of primary magmatic concentrations (Sun and Nesbitt 1978; Lahaye and Arndt 1996).

8.2. Crustal contamination

The ascent of the komatiitic magma through the continental lithosphere to the surface makes crustal contamination inevitable, either through assimilation–fractional crystallization (AFC) or thermal erosion of floor rocks, due to their higher liquidus temperature (Halama *et al.* 2004; Tang *et al.* 2012). Sylvester *et al.* (1997) pioneered the use of Nb/Th ratios in Archaean basalts as a monitor of the extent and timing of extraction of continental crust from the mantle. The primitive

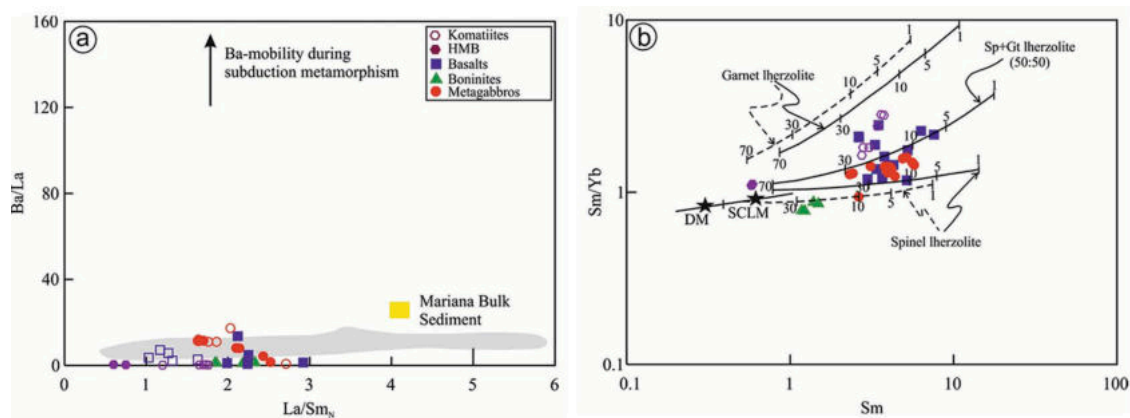


Figure 8. (a) Variation of Ba/La with $(La/Sm)_N$ (after Ghatak *et al.* 2012). (b) Sm/Yb vs. Sm diagram for the meta-basalts. Modelling results of mantle melting with different starting materials (garnet–lherzolite, garnet–spinel lherzolite, and spinel–lherzolite) are shown, based on the non-batch melting equations of Shaw (1970). The dashed and solid lines are the melting trends for depleted mantle (DM, Sm = 0.3 ppm and Sm/Yb = 0.86, McKenzie and O’Nions 1991) and enriched subcontinental lithospheric mantle (SCLM, Sm = 0.6 ppm and Sm/Yb = 0.96, Aldanmaz *et al.* 2000), respectively. Partition coefficients used in the modelling are from McKenzie and O’Nions (1991). The numbers beside the lines are degrees of partial melting for a given mantle source.

mantle has a Nb/Th ratio of 8, Archaean continental crust proxied by tonalites has a value of 0.76, and Phanerozoic upper continental crust a value of 1.1 (Sun and McDonough 1989; Rudnick and Gao 2003; Condie 2005). Nb/Th value of the studied komatiites varies between 6 and 7. They neither show LREE enrichment nor negative Nb anomalies on the primitive mantle-normalized diagram. Further, they are characterized by the Zr/Hf and Zr/Th ratios in the range similar to those of primitive mantle. Collectively, these features of the studied komatiites rule out the possibility of crustal contamination. Also supporting this argument are the Ti/Zr and Nb/La ratios which are close to recommended values for mantle (Hoffman 1988). Moreover, the pillow structure of these komatiites suggests a marine environment rather than a continental setting for their eruption. However, three of the komatiitic basalts exhibit Nb/Th values less than 3, and are characterized by very weak or no Zr negative anomalies coupled with Nb–Ta negative anomalies and enriched LREE, all of which suggests probable crustal contamination *en route* to the surface.

Contrarily, the Nb/Th values of 2–4 for majority of the basalts and 1–3 for the associated gabbros suggest crustal contamination incurred by these litho units. Contamination of these litho units by the older sialic crustal basement *en route* to the surface is a possibility, given that these litho units unconformably overlie basement gneisses (Peninsular Gneisses). Alternatively, contamination of the magma source of the studied basalts and gabbros due to interaction of mantle plumes with metasomatized continental mantle lithosphere also

cannot be ruled out. Said *et al.* (2012) have demonstrated, based on their study of Nb/Th ratios in komatiites and associated tholeiitic basalts of the Kalgoorlie terrane specifically and the larger Eastern Goldfields super-terrane more generally, that the contamination by subduction-metasomatized mantle lithosphere dominates due to interaction of mantle plumes with the base of the lithosphere than crustal contamination. Moreover, all the analysed samples of basalts and gabbros exhibit negative Nb–Ta anomalies implying assimilation of subduction-processed lithospheric mantle material by plume derived magma (Song *et al.* 2008). However, in the absence of radiogenic isotope data, it is suggested that the possibility of contamination by continental crust and subduction-metasomatized sub-continental lithospheric mantle cannot be ruled out.

Phanerozoic boninites occur in oceanic suprasubduction zone ophiolites, dominantly forearcs (Angerer *et al.* 2013 and references therein). However, their Archaean counterparts are found in intraoceanic arcs associated with primitive island arc tholeiites (Polat and Kerrich 2006). The characteristic features of continental lithosphere, viz. LREE enrichment and Nb/Th < 8, exhibited by boninites of WGB makes it difficult to establish whether they were erupted in an oceanic or continental margin setting. Though, contamination of a refractory mantle melt with felsic crust, unrelated to an intraoceanic arc setting, is accounted for the formation of Archaean boninite-like magmas (Smithies 2002; Angerer *et al.* 2013), it fails to explain the U-shaped REE patterns, for Archaean continental crust does not have negatively fractionated HREE (Taylor and

McLennan 1985). Given the U-shaped REE patterns and negative Zr–Hf anomalies of the boninites of the present study, which are not observed in Archaean continental crust or any other volcanic lithologies, it is suggested that the contamination is minimal.

8.3. Nature and composition of mantle sources and melting conditions

8.3.1. Komatiites

Experimental studies (Ohtani *et al.* 1989; Herzberg 1999) have shown that Al-depleted komatiites are generated by partial melting of peridotite at pressures greater than 8 GPa, whilst Al-undepleted komatiites have been explained by high degree melting of peridotite at shallow level in mantle. Komatiites of the present study have CaO/Al₂O₃ ratio less than 1, but feature high MgO (>20 wt%) content and (Gd/Yb)_N ratio (1.27–1.28). Moreover, hydrous alteration lowers the CaO content in volcanic rocks resulting in lower CaO/Al₂O₃ ratios (Chikhaoui 1981). Such mechanisms of post-magmatic hydrothermal alteration is accounted here for the observed lower values of CaO/Al₂O₃ ratios of the komatiites, despite their high MgO, low Al₂O₃/TiO₂ and higher (Gd/Yb)_N values. Chondritic REE ($\Sigma\text{REE} = 8.05\text{--}8.35$ ppm) and LREE depletion [(La/Sm)_N = 0.60–0.75] of the studied komatiites is consistent with a depleted mantle source. Fan and Kerrich (1997) used Zr and Hf anomalies have been used to constrain the nature of sources and melt residues. WGB komatiites exhibit slight to moderate Zr and Hf anomalies in primitive mantle-normalized spider diagrams (Figure 6(b)), implying their derivation from a deep (~350–250 km) mantle source where garnet fractionated or was retained in the residue (cf. Fan and Kerrich 1997). Strong negative Nb anomalies on the primitive mantle-normalized multi element diagram have been accounted for magma generation at shallower mantle in arc environments or even crustal contamination processes (Polat and Kerrich 2000). Contrarily, positive Nb anomalies have been attributed to magma generation from plume source that contain recycled slab material at greatest mantle depths (Kerrich and Xie 2002). Lack of Nb anomalies and/or positive Nb anomalies in komatiites in Sargur Group greenstone sequences in WDC have been interpreted to be derived from mantle plume containing recycled slab component (Jayananda *et al.* 2008), which is also substantiated by earlier episodes of crustal growth in arc settings (Naqvi *et al.* 2009). Komatiites of the present study show either zero or slight negative Nb anomalies on primitive mantle-normalized diagram (Figure 6(b)) implying magma generation from a plume source possibly involving minor crustal contamination of the rising plume. Al-

depleted nature of the studied komatiites suggests that they were generated by partial melting of depleted mantle source at greater depths (~350–250 km) with pressure exceeding 8 GPa.

8.3.2. HMB, basalts, and associated gabbros

Enrichment of LILE and HFSE in the HMB, basalts, and associated gabbros of WGB implies that they were derived from an enriched mantle source. They exhibit pronounced negative Nb–Ta anomalies in the primitive mantle-normalized multi-element diagrams (Figure 6(d, f, j)), which differs them from plume-related or asthenosphere-derived magmas that have trace element pattern similar to OIB/MORB. The probability of crustal contamination for the observed negative Nb–Ta anomalies in HMB (except two samples), basalts and five of the gabbros is ruled out owing to the fact that the pronounced negative Zr and Hf anomalies of these rock types in the primitive mantle normalized multi-element diagram argues against it, for crustal contamination enriches the Zr and Hf concentration. Either metasomatism by melts/fluids released from the subducting slab (Maury *et al.* 1992) or interaction between lithospheric mantle and volatile-rich, low-density melts originated from the asthenosphere (McKenzie 1989; Gibson *et al.* 1995) are the possible models responsible for the formation of the enriched mantle source. However, majority of the gabbros and two of the HMB have zero or slight positive Zr anomalies indicating crustal contamination. Considering the significant negative Nb, Ta, and Ti anomalies of the crustally uncontaminated HMB, basalts and gabbros of WGB in primitive mantle-normalized multi-element diagram, we believe the enrichment of the mantle source beneath the WGB was due to subduction modified continental lithospheric mantle source. This consideration is also supported by uniform enrichment of Th–U over Nb–Ta, and relatively high La/Nb (1.27–5.76) and La/Ta (22–74) ratios of HMB, basalts, and gabbros, which are typical of a subduction-modified mantle source (Thompson and Morrison 1988; Saunders *et al.* 1992).

REE abundances and ratios are widely used to determine the origin of the mantle magmas and to infer the mantle melting (Aldanmaz *et al.* 2000; Zhao and Zhou 2007; Liu *et al.* 2012). Sm/Yb ratio can be a useful tool to constrain the mantle source mineralogy, for Sm, being an incompatible element, is affected significantly by variation in the source mineralogy (e.g. garnet or spinel), whereas Yb is compatible with garnet but not with clinopyroxene or spinel (Aldanmaz *et al.* 2000). Sm/Yb ratios of spinel–lherzolite source partial melts are similar to those of mantle, and thus form a horizontal melting trend that lies within, or close to, a mantle array defined

by depleted mantle (DM, McKenzie and O'Nions 1991) and enriched subcontinental lithospheric mantle (SCLM, Aldanmaz *et al.* 2000). On the other hand, partial melts from a garnet–lherzolite source (with garnet residue) will have significantly higher Sm/Yb ratios than mantle source. HMB, basalts and gabbros of WGB have Sm/Yb ratios higher than spinel–lherzolite melting curve, but lower than the garnet–lherzolite melting trend (Figure 8 (b)) implying a mantle source of spinel-bearing garnet–lherzolite. Our modelling suggests that a degree of 5–30% partial melting of such a mantle source is needed for the generation of the parent magma of the studied HMB, basalts and gabbros (Figure 8(b)). Further, relatively low Ce/Y ratios (<2) suggest that they were generated within the spinel–garnet stability at a depth of approximately 60–80 km (McKenzie and Bickle 1988).

8.3.3. Boninites

The WGB of boninites are characterized by high MgO (13.73–14.73 wt.%), low TiO₂ (0.35–0.39 wt.%) contents, high Al₂O₃/TiO₂ (29–32), and low (Gd/Yb)_N ratios (<1) with enrichment in Ni, Cr, LREE, depletion in MREE compared to LREE and HREE and distinct negative anomalies at Nb, Ta, Zr, Hf, and Ti on primitive mantle-normalized multi-element diagram. The REE and incompatible systematics of these boninites resemble more of basalts of the WGB, implying that they were derived from the same source as that of basalts. The pronounced Nb–Ta and Zr–Hf negative anomalies in the primitive mantle-normalized multi-element diagram, similar to that of studied basalts, suggest that they had subduction-modified mantle source. However, unlike basalts, they fall on the spinel–lherzolite trend line in the Sm versus Sm/Yb binary plot (Figure 8(b)), implying a 20–30% partial melting of spinel–lherzolite mantle source is responsible for their generation.

8.4. Geodynamic implications

8.4.1. Plume characteristics

Lateral accretion of crust in the subduction zone setting is accounted for the formation of continental crust of TTG composition and in large part for the general granodioritic composition of the Archaean continental crust (Taylor and McLennan 1985). Drury (1983) proposed an arc setting to explain the origin of mafic volcanics of the WDC. This model, however, has been widely argued against as it cannot account for some of the observed chemical characteristics, particularly Al-depletion, zero or positive Nb anomalies, Nb/U, Nb/Th, Nb/La, Th/U ratios, and the higher eruption temperatures (~1600°C) in the komatiites. Consequently, these geochemical

characteristics of komatiites are not consistent with an arc environment. Further, high-MgO, Al-depletion, low incompatible element contents together with higher eruption temperatures (1600–1700°C) of the ultramafic rocks is considered to reflect a mantle melting at high temperatures at greater depths, probably in the hottest portion of ascending mantle plumes (cf. Jayananda *et al.* 2008). The studied komatiites feature higher contents of MgO, Ni and Cr, Al-depletion, and zero or negligible Nb-anomalies, all of which argues in favour of their generation in a deep mantle hot spot environment associated with a rising plume. However, a plume model alone does not account for the geochemical characteristics of HMB, basalts-gabbros, and boninites of the WGB.

8.4.2. Subduction signatures

Partial melting of metasomatized mantle wedge is held responsible for the observed relative enrichment of LILE and LREE with pronounced HFSE depletion in arc magmas (McCulloch and Gamble 1991; Pearce *et al.* 2000). Accordingly, the sub-arc mantle wedge and fluids/melts derived from dehydrated subducted slab are potential contributors to arc magma sources, and their influence on subduction zone magmatism can be identified using distinct geochemical fingerprints preserved in the volcanic rocks (Perfit *et al.* 1980; Pearce and Peate 1995; Maruyama *et al.* 2009). HMB of the WGB exhibit slightly enriched LREE patterns compared to komatiite, and have lower magnitudes of negative anomalies at Nb, Zr, Hf, and Ti, whereas basalts and gabbros exhibit pronounced negative Nb, Ta, Zr, Hf, and Ti anomalies and differentially enriched LREE patterns (Figure 6(d,f,j)). All the three rock types display relative depletion of HFSE and HREE with respect to LILE and LREE, manifested in terms of LILE/HFSE and LREE/HFSE ratios. All these features suggest arc magmatism in a subduction zone setting (Pearce 2008). This conclusion is also manifested in Figure 9, in which the HMB, basalts and gabbros indicate their arc affinity.

Similarly, boninites are erupted during the early stages of subduction and carry distinct signatures of interaction between mantle wedge and subducting slab (Kusky *et al.* 2013; Zhou *et al.* 2014). Boninite magmatism requires (1) addition of hydrous fluids to the refractory mantle peridotite, which lowers the solidus temperature and generate partial melting, and (2) high temperature (1150–1350°C) at shallow depth (<50 km) in a subduction zone environment (Crawford *et al.* 1989; Polat *et al.* 2002; Smithies 2002). For arc magmas, it has been shown that there is a relationship between the geochemistry and the thermal structure of subduction zones (see

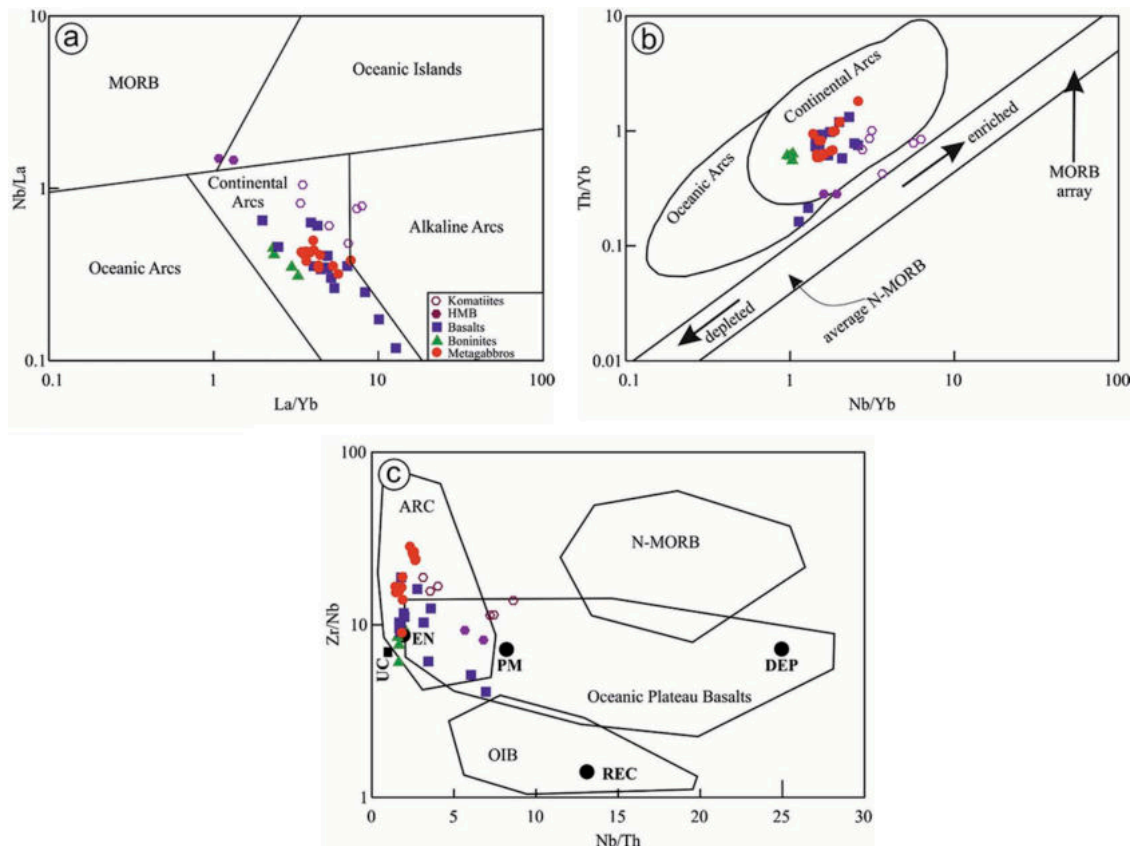


Figure 9. (a) La/Yb vs. Nb/La plot of Hollocher et al. (2012) and (b) Nb/Yb vs. Th/Yb plot of Pearce and Peate (1995) showing continental arc affinity for the HMB, basalts, boninites, and metagabbros. Komatiites show oceanic arc/island and MORB affinity. (c) Nb/Th vs. Zr/Nb plot of Condie (2005). PM: primitive mantle; DM: depleted mantle; OIB: oceanic island basalts; N-MORB: normal mid-oceanic ridge basalts; REC: recycled component; ARC: arc related basalts; EN: enriched component; UC: upper continental crust.

Defant and Drummond 1990). It is commonly believed that boninites originate in the sub-arc mantle wedge during the subduction of young, hot oceanic lithosphere (Tatsumi and Maruyama 1989; Stern et al. 1991; Pearce et al. 1992). Under these conditions, the subducting slabs are likely to undergo melting rather than dehydration to produce high-MgO magmas, including low-Ti tholeiites and boninites (Drummond et al. 1996). As discussed earlier (Section 8.3.3), boninites of WGB have been generated by the partial melting of similar source as those of the studied basalts, but at shallow depth in a subduction zone environment. Figure 10 attests for their arc affinity, which is also corroborated by their pronounced Nb–Ta and Zr–Hf negative anomalies, LREE enrichment, and HREE depletion.

8.4.3. Implications

According to the established stratigraphy of WGB, the metabasalts of the Kudremukh Formation, interleaved with chloritic schists (probably representing basic tuffs),

sparse quartzites and metagabbroic sills, rests unconformably upon older gneisses (Ramakrishnan and Harinadha Babu 1981). Basal quartz-pebble conglomerates (*Walkunje Conglomerates* – equivalent of *Kartikere Conglomerates* of Bababudan greenstone belt) separate this metabasalts of Kudremukh Formation from the basement gneisses, and is locally well developed near Walkunje village in the southwestern margin of the WGB. Accordingly, Ramakrishnan and Harinadha Babu (1981) considered that this metabasalts are equivalents of the metavolcanics of *Santevari Formation* (~2.7 Ga) of Bababudan belt. The studied komatiites of WGB belongs to Palaeoarchaeon Sargur Group (3.1–3.3 Ga) and occurs as enclaves within the Peninsular Gneiss with a strike length of over 1 km. Though the exact timing of their eruption is not yet known, it can be presumed to be somewhere around 3.1–3.3 Ga (i.e. age of Sargur Group). Whether these komatiites are contemporaneous to Peninsular Gneiss, as is the case suggested by Jayananda et al. (2008) for the komatiites of Sargur Group elsewhere in the greenstone belts of WDC is yet to be determined. The studied komatiites, which occurs at the

base of the WGB probably represent the remnants of ancient oceanic crust, which got juxtaposed along with the metabasalts in between the gneissic continental crusts. The sheared tectonic contact between the basement gneiss and the greenstones (Dharwar Supergroup of rocks) supports this argument.

Our study has indicated that the komatiites and HMB–basalts–boninites were formed in a distinct geodynamic setting. The elemental data of the studied komatiites, particularly depleted LREE do not show any involvement of older crust in their genesis or significant crustal contamination. It appears that plume, that had been initiated beneath the oceanic crust far from sizable ancient continental land mass (Figure 10(a)) somewhere around ≥ 3.0 Ga, has given rise to WGB komatiites. The pillow structures of these komatiites indicate their eruption in oceanic environments. Later, somewhere around 2.8–2.7 Ga, boninites were formed during the initial stages of subduction of the komatiitic laden oceanic crust beneath the gneissic continental crust. Further subduction of down-going oceanic crust has resulted in the differential melting at variable depths in a subduction related arc-setting (Figure 10(b,c)) and emplacement of HMB and basalts on a continental margin around 2.8–2.7 Ga. The occasional gabbros, which form the sills within the basaltic unit might have been emplaced in small volumes within the weak zones of basalts during subduction process.

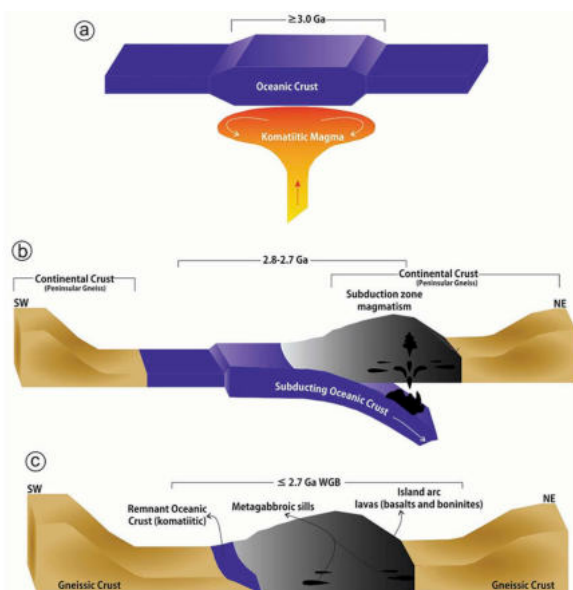


Figure 10. Cartoon showing plume-arc model for the formation of komatiites, high-magnesium basalt (HMB), basalts, boninites, and metagabbros of Western Ghats belt (WGB) in western Dharwar Craton (WDC).

9. Conclusions

The WGB, one of the largest greenstone belts in WDC, predominantly contains a variety of ultramafic–mafic volcanic rocks with associated metagabbros, which are suggested to be generated during different stages of crustal growth process. Komatiitic magmas were derived by melting of depleted upper mantle sources at different depths with or without garnet in the residue. The existence of a depleted mantle reservoir at ≥ 3.0 Ga probably indicates that the upper mantle had already lost a melt component during the early Archaean (>3.3 Ga) crustal growth through a preceding greenstone-TTG cycle. HMB, basalts, boninites and associated gabbros are the products of arc magmatism. The REE chemistry of the HMB, basalts, boninites, and gabbros attests to a gradual transition in melting depth varying between spinel and garnet stability field in an arc regime. The close spatial association but contrasting elemental characteristics of komatiites and HMB–basalts–boninites, can be best explained by a plume-arc model, in which the 3.0 Ga komatiites are considered to be the products of plume volcanism in an oceanic plateau setting, while the HMB, basalts, boninites, and associated gabbros were emplaced in a continental margin setting around 2.8–2.7 Ga.

Acknowledgements

Trivikram Manuvachari and Sampathkumar Talwar were of great help during the field work. J. P. Oldra is thanked for sample preparation. C. Liorzou and B. Gueguen are thanked for their assistance during analytical work. The Chairman, Department of Studies in Geology, Karnatak University, Dharwad is thanked for providing infrastructural facilities to carry out the present study.

Disclosure statement

No potential conflict of interest was reported by the authors.

ORCID

Chandan-Kumar B <http://orcid.org/0000-0002-7126-544X>

References:

- Aldanmaz, E., Pearce, J., Thirlwall, M., and Mitchell, J., 2000, Petrogenetic evolution of late Cenozoic, post-collision volcanism in western Anatolia, Turkey: *Journal Volcanol Geotherm Researcher*, v.102, p.67–95. [10.1016/S0377-0273\(00\)00182-7](https://doi.org/10.1016/S0377-0273(00)00182-7).
- Angerer, T., Kerrich, R., and Hagemann, S.G., 2013, Geochemistry of a komatiitic, boninitic, and tholeiitic basalt association in the Mesoarchean Koolyanobbing greenstone belt, Southern Cross Domain, Yilgarn craton: Implications for mantle sources and geodynamic setting of banded iron

- formation: *Precambrian Research*, v.224, p.110–128. [10.1016/j.precamres.2012.09.012](https://doi.org/10.1016/j.precamres.2012.09.012).
- Arndt, N.T., 1994, *Archaean Komatiites*, Condie, K.C., Ed., *Archaean crustal evolution*, Elsevier, Amsterdam, 11–44.
- Arndt, N.T., Leshner, C.M., and Barnes, S.J., 2008, *Komatiites*, Cambridge University Press, New York.
- Arndt, N.T., and Nisbet, E.G., 1982, *Komatiites*: London, George Allen and Unwin Publication.
- Balakrishnan, S., Hanson, G.N., and Rajamani, V., 1991, Pb and Nd isotope constraints on the origin of high Mg and tholeiitic amphibolites, Kolar Schist Belt, South India: *Contributions to Mineral Petrol*, v.107, p.279–292. [10.1007/BF00325099](https://doi.org/10.1007/BF00325099).
- Balakrishnan, S., Rajamani, V., and Hanson, G.N., 1999, U–Pb ages for zircon and titanite from the Ramagiri area, Southern India: Evidence for accretionary origin of eastern Dharwar craton during late archean: *The Journal of Geology*, v.107, p.69–86. [10.1086/314331](https://doi.org/10.1086/314331).
- Balasubramanyam, M.N., Bishui, P.K., Chandy, K.C., Gupta, S.N., Jana, N.K., Paul, D.K., and Prasad, R., 1982, New Rb–Sr age of Kanara granite, South Kanara district, Karnataka State: *Journal of Geological Society of India*, v. 23, p. 402–405.
- Balasubramanyam, M.N., 1978, *Geochronology and geochemistry of Archean tonalitic gneisses and granites of South Kanara district*, Windley, B.F., and Naqvi, S.M., Eds., *Archaean Geochemistry*, Elsevier, Karnataka State, India, 57–77.
- Barrat, J.A., Yamaguchi, A., Greenwood, R.C., Benoit, M., Cotten, J., Bohn, M., and Franchi, I.A., 2008, Geochemistry of diogenites: Still more diversity in their parental melts: *Meteorit Planet Sciences*, v.43, p.1759–1775. [10.1111/j.1945-5100.2008.tb00641.x](https://doi.org/10.1111/j.1945-5100.2008.tb00641.x).
- Barrat, J.A., Yamaguchi, A., Greenwood, R.C., Bohn, M., Cotten, J., Benoit, M., and Franchi, I.A., 2007, The Stannern trend eucrites: contamination of main group eucritic magmas by crustal partial melts: *Geochimica Et Cosmochimica Acta*, v.71, p.4108–4124. [10.1016/j.gca.2007.06.001](https://doi.org/10.1016/j.gca.2007.06.001).
- Barrat, J.A., Zanda, B., Moynier, F., Bollinger, C., Liorzou, C., and Bayon, G., 2012, Geochemistry of CI chondrites: Major and trace elements, and Cu and Zn Isotopes: *Geochimica Et Cosmochimica Acta*, v.83, p.79–92. [10.1016/j.gca.2011.12.011](https://doi.org/10.1016/j.gca.2011.12.011).
- Benn, K., Mareschal, J.-C., and Condie, K.C., Eds., 2013, *Archean geodynamics and environments*, *Geophysical Monograph Series*, American Geophysical Union, Washington, D. C.
- Brown, A.V., and Jenner, G.A., 1989, Geological setting, petrology and chemistry of Cambrian boninite and low-Ti tholeiites lavas in Western Tasmania, Crawford, A.J., Ed., *Boninites and Related Rocks*, Unwin Hyman, London, 232–263.
- Chadwick, B., Vasudev, V.N., and Hegde, G.V., 2000, The Dharwar craton, southern India, interpreted as the result of Late Archaean oblique convergence: *Precambrian Research*, v.99, p.91–111. [10.1016/S0301-9268\(99\)00055-8](https://doi.org/10.1016/S0301-9268(99)00055-8).
- Chadwick, B., Vasudev, V.N., and Hegde, G.V., 2003, The chitradurga schist belt and its adjacent plutonic Rocks, NW of Thngabhadra, Karnataka: A duplex in the late archaean convergent setting of the dharwar craton: *Journal of Geological Society of India*, v. 61, p. 645–663.
- Chadwick, B., Vasudev, V.N., Hegde, G.V., and Nutman, A.P., 2007, Structure and SHRIMP U/Pb zircon ages of granites adjacent to the chitradurga schist belt: implications for Neoproterozoic Convergence in the Dharwar Craton, Southern India: *Journal of Geological Society of India*, v. 69, p. 5–24.
- Chalapathi Rao, N.V., Creaser, R.A., Lehmann, B., and Panwar, B. K., 2013, Re–Os isotope study of Indian kimberlites and lamproites: Implications for mantle source regions and cratonic evolution: *Chemical Geology*, v.353, p.36–47. [10.1016/j.chemgeo.2012.12.013](https://doi.org/10.1016/j.chemgeo.2012.12.013).
- Charan, S.N., Naqvi, S.M., and Ramesh, S.L., 1988, Geology and geochemistry of spinifex-textured peridotitic komatiite from mayasandra schist belt, Karnataka: *Journal of Geological Society of India*, v. 32, p. 343–350.
- Chardon, D., Jayananda, M., Chetty, T.R.K., and Peucat, -J.-J., 2008, Precambrian continental strain and shear zone patterns: South Indian case: *Journal of Geophysical Research*, v.113, p.B08402. [10.1029/2007JB005299](https://doi.org/10.1029/2007JB005299).
- Chardon, D., Jayananda, M., and Peucat, -J.-J., 2011, Lateral constrictional flow of hot orogenic crust: Insights from the Neoproterozoic of south India, geological and geophysical implications for orogenic plateaux. *Geochemistry, Geophys: Geosystems*, v. 12, p. 1–24.
- Chardon, D., Peucat, -J.-J., Jayananda, M., Choukroune, P., and Fanning, C.M., 2002, Archean granite-greenstone tectonics at Kolar (South India): Interplay of diapirism and bulk inhomogeneous contraction during juvenile magmatic accretion: *Tectonics*, v.21, [10.1029/2001TC901032](https://doi.org/10.1029/2001TC901032).
- Chikhaoui, M., 1981, Les roches volcaniques du proterozoique superieur de la chaine pan-Africaine dans le NW de l' Afrique (Hoggar, Anti-Atlas, Adrar des Iforas): *Caracterisation geochimique et mineralogique, implications geodynamiques*, These d' Etat, Montpellier.
- Condie, K.C., 1981, *Archean Greenstone Belts*, Elsevier, Amsterdam.
- Condie, K.C., 2005, High field strength element ratios in Archean basalts: A window to evolving sources of mantle plumes?: *Lithos*, v.79, p.491–504. [10.1016/j.lithos.2004.09.014](https://doi.org/10.1016/j.lithos.2004.09.014).
- Cotten, J., Le Dez, A., Bau, M., Caroff, M., Maury, R.C., Dulski, P., Fourcade, S., Bohn, M., and Brousse, R., 1995, Origin of anomalous rare-earth element and yttrium enrichments in subaerially exposed basalts: Evidence from French Polynesia: *Chemical Geology*, v.119, p.115–138. [10.1016/0009-2541\(94\)00102-E](https://doi.org/10.1016/0009-2541(94)00102-E).
- Crawford, A.J., Falloon, T.J., and Green, D.H., 1989, Classification, petrogenesis and tectonic setting of boninites, Crawford, A.J., Ed., *Boninites and Related Rocks*, Unwin Hyman, London, 2–49.
- Defant, M.J., and Drummond, M.S., 1990, Derivation of some modern arc magmas by melting of young subducted lithosphere: *Nature*, v.347, p.662–665. [10.1038/347662a0](https://doi.org/10.1038/347662a0).
- Devaraju, T.C., Viljoen, R.P., Sawkar, R.H., and Sudhakara, T.L., 2009, Mafic and ultramafic magmatism and associated mineralization in the Dharwar Craton, southern India: *Journal of Geological Society of India*, v.73, p.73–100.
- Dey, S., Nandy, J., Choudhary, A.K., Liu, Y., and Zong, K., 2013, Neoproterozoic crustal growth by combined arc-plume action: Evidence from the Kadiri Greenstone Belt, eastern Dharwar craton, India. *Geol. Soc. London, Spec: Publ*, v. 389, p. 135–163.
- Dostal, J., Mueller, W.U., and Murphy, J.B., 2004, Archean Molasse Basin Evolution and Magmatism, Wabigoon Subprovince, Canada: *The Journal of Geology*, v.112, p.435–454. [10.1086/421073](https://doi.org/10.1086/421073).

- Drummond, M.S., Defant, M.J., and Kepezhinskas, P.K., 1996, Petrogenesis of slab-derived trondhjemite-tonalite-dacite/adakite magmas: Geological Society of America Special Papers, v. 315, p. 205–215.
- Drury, S.A., 1981, Geochemistry of Archaean metavolcanic rocks from the Kudremukh area, Karnataka: Journal of Geological Society of India, v. 22, p. 405–416.
- Drury, S.A., 1983, The petrogenesis and setting of Archaean metavolcanics from Karnataka State, South India: *Geochimica Et Cosmochimica Acta*, v.47, p.317–329. [10.1016/0016-7037\(83\)90144-8](https://doi.org/10.1016/0016-7037(83)90144-8).
- Drury, S.A., and Holt, R.W., 1980, The tectonic framework of the south Indian craton: A reconnaissance involving Landsat imagery: *Tectonophysics*, v.65, p.T1–T15. [10.1016/0040-1951\(80\)90073-6](https://doi.org/10.1016/0040-1951(80)90073-6).
- Drury, S.A., Holt, R.W., Van Calsteren, P.C., and Beckinsale, R.D., 1983, Sm-Nd and Rb-Sr ages for Archaean rocks from western Karnataka, South India: *Journal of Geological Society of India*, v. 24, p. 454–459.
- Fan, J., and Kerrich, R., 1997, Geochemical characteristics of Al-depleted and undepleted komatiites and HREE-enriched tholeiites, western Abitibi greenstone belt: Variable HFSE/REE systematics in a heterogeneous mantle plume: *Geochimica Et Cosmochimica Acta*, v.61, p.4723–4744. [10.1016/S0016-7037\(97\)00269-X](https://doi.org/10.1016/S0016-7037(97)00269-X).
- Ganguly, S., Manikyamba, C., Saha, A., Lingadevaru, M., Santosh, M., Rambabu, S., Khelen, A.C., Purushotham, D., and Linga, D., 2016, Geochemical characteristics of gold bearing boninites and banded iron formations from Shimoga greenstone belt, India: Implications for gold genesis and hydrothermal processes in diverse tectonic settings: *Ore Geology Reviews*, v.73, p.59–82. [10.1016/j.oregeorev.2015.10.013](https://doi.org/10.1016/j.oregeorev.2015.10.013).
- Ghatak, A., Basu, A.R., and Wakabayashi, J., 2012, Elemental mobility in subduction metamorphism: Insight from metamorphic rocks of the Franciscan Complex and the Feather River ultramafic belt, California: *International Geology Reviews*, v.54, p.654–685. [10.1080/00206814.2011.567087](https://doi.org/10.1080/00206814.2011.567087).
- Gibson, S.A., Thompson, R.N., Leonardos, O.H., Dickin, A.P., and Mitchell, J., 1995, The Late Cretaceous Impact of the Trindade Mantle Plume: Evidence from Large-volume, Mafic, Potassic Magmatism in SE Brazil: *Journal Petrol*, v.36, p.189–229. [10.1093/petrology/36.1.189](https://doi.org/10.1093/petrology/36.1.189).
- Halama, R., Marks, M., Brüggmann, G., Siebel, W., Wenzel, T., and Markl, G., 2004, Crustal contamination of mafic magmas: Evidence from a petrological, geochemical and Sr–Nd–Os–O isotopic study of the Proterozoic Isortoq dike swarm, South Greenland: *Lithos*, v.74, p.199–232. [10.1016/j.lithos.2004.03.004](https://doi.org/10.1016/j.lithos.2004.03.004).
- Herzberg, C., 1999, Phase equilibrium constraints on the formation of cratonic mantle, Fie, Y., Bertka, C.M., and Mysen, B.O., Eds., *Mantle Petrology: Michigan, Field Observations and High-Pressure Experimentation*, Geochemical Society (Special Publication, 241–257).
- Hoffman, A.W., 1988, Chemical differentiation of the Earth: The relationship between mantle, continental crust and oceanic crust: *Earth and Planetary Science Letters*, v.90, p.297–314. [10.1016/0012-821X\(88\)90132-X](https://doi.org/10.1016/0012-821X(88)90132-X).
- Hollocher, K., Robinson, P., Walsh, E., and Roberts, D., 2012, Geochemistry of amphibolite-facies volcanics and gabbros of the storen nappe in extensions west and southwest of trondheim, western gneiss region, norway: a key to correlations and paleotectonic settings, v. 312, p 4. doi:[10.2475/04.2012.01](https://doi.org/10.2475/04.2012.01). 357–416
- Irvine, T.N., and Baragar, W.R.A., 1971, A guide to the chemical classification of the common volcanic rocks: *Canada Journal Earth Sciences*, v.8, p.523–548. [10.1139/e71-055](https://doi.org/10.1139/e71-055).
- Iyer, G.V.A., and Vasudev, V.N., 1979, Geochemistry of the Archaean Metavolcanic Rocks of Kolar and Hutti Gold Fields, Karnataka, India: *Journal of Geological Society of India*, v. 20, p. 419–432.
- Jafri, S.H., Rao, D.V.S., Ahmad, S.M., and Mathur, R., 1997, Spinifex Textured Peridotitic Komatiite from Nuggihalli and R.N. Pur Schist Belts, Karnataka. *Journal of Geological Society of India*, v. 49, p. 33–38.
- Jayananda, M., Banerjee, M., Pant, N.C., Dasgupta, S., Kano, T., Mahesha, N., and Mahabaleswar, B., 2011, 2.62 Ga high-temperature metamorphism in the central part of the Eastern Dharwar Craton: Implications for late Archaean tectonothermal history: *Geological Journal*, v.47, p.213–236. [10.1002/gj.1308](https://doi.org/10.1002/gj.1308).
- Jayananda, M., Chardon, D., Peucat, -J.-J., and Fanning, C.M., 2015, Paleo- to Mesozoic TTG accretion and continental growth in the western Dharwar craton, Southern India: Constraints from SHRIMP U–Pb zircon geochronology, whole-rock geochemistry and Nd–Sr isotopes: *Precambrian Research*, v.268, p.295–322. [10.1016/j.precamres.2015.07.015](https://doi.org/10.1016/j.precamres.2015.07.015).
- Jayananda, M., Kano, T., Peucat, J., and Channabasappa, S., 2008, 3.35Ga komatiite volcanism in the western Dharwar craton, southern India: Constraints from Nd isotopes and whole-rock geochemistry: *Precambrian Research*, v.162, p.160–179. [10.1016/j.precamres.2007.07.010](https://doi.org/10.1016/j.precamres.2007.07.010).
- Jayananda, M., Moyen, J.-F., Martin, H., Peucat, -J.-J., Auvray, B., and Mahabaleswar, B., 2000, Late Archaean (2550–2520 Ma) juvenile magmatism in the Eastern Dharwar craton, southern India: Constraints from geochronology, Nd–Sr isotopes and whole rock geochemistry: *Precambrian Research*, v.99, p.225–254. [10.1016/S0301-9268\(99\)00063-7](https://doi.org/10.1016/S0301-9268(99)00063-7).
- Jayananda, M., Peucat, -J.-J., Chardon, D., Rao, B.K., Fanning, C.M.M., and Corfu, F., 2013a, Neoproterozoic greenstone volcanism and continental growth, Dharwar craton, southern India: Constraints from SIMS U–Pb zircon geochronology and Nd isotopes: *Precambrian Research*, v.227, p.55–76. [10.1016/j.precamres.2012.05.002](https://doi.org/10.1016/j.precamres.2012.05.002).
- Jayananda, M., Tsutsumi, Y., Miyazaki, T., Gireesh, R.V., Kapfo, K., Hidaka, H., and Kano, T., 2013b, Geochronological constraints on Meso- and Neoproterozoic regional metamorphism and magmatism in the Dharwar craton, southern India: *Journal Asian Earth Science*, v.78, p.18–38. [10.1016/j.jseas.2013.04.033](https://doi.org/10.1016/j.jseas.2013.04.033).
- Jensen, L.S., 1976, A new method of classifying alkali volcanic rocks, Ontario Division Mines Miscellaneous Paper 66.
- Kerrich, R., and Xie, Q., 2002, Compositional recycling structure of an Archaean super-plume: Nb–Th–U–LREE systematics of Archaean Komatiites and basalts revisited: *Contributions to Mineral Petrol*, v.142, p.476–484. [10.1007/s004100100301](https://doi.org/10.1007/s004100100301).
- Khan, R.M.K., Charan, S.N., Arora, M., and Naqvi, S.M., 1995, Mineral composition and its bearing on depositional history of BIF of Kudremukh Schist Belt, Karnataka: *Journal Geological Society India*, v. 46, p. 603–610.
- Khan, R.M.K., Govil, P.K., and Naqvi, S.M., 1992, Geochemistry and genesis of banded iron formation from Kudremukh

- schist belt, Karnataka Nucleus, India: *Journal of Geological Society of India*, v. 40, p. 311–328.
- Krogstad, E.J., Hanson, G.N., and Rajamani, V., 1991, U-Pb Ages of zircon and sphene for two gneiss terranes adjacent to the kolar schist belt, South India: evidence for separate crustal evolution histories: *The Journal of Geology*, v.99, p.801–815.[10.1086/629553](https://doi.org/10.1086/629553).
- Kröner, A., 1991, Tectonic evolution in the Archaean and Proterozoic: *Tectonophysics*, v.187, p.393–410.[10.1016/0040-1951\(91\)90478-B](https://doi.org/10.1016/0040-1951(91)90478-B).
- Kusky, T.M., Windley, B.F., Safonova, I., Wakita, K., Wakabayashi, J., Polat, A., and Santosh, M., 2013, Recognition of ocean plate stratigraphy in accretionary orogens through Earth history: A record of 3.8 billion years of sea floor spreading, subduction, and accretion: *Gondwana Research*, v.24, p.501–547.[10.1016/j.gr.2013.01.004](https://doi.org/10.1016/j.gr.2013.01.004).
- Lahaye, Y., and Arndt, N.T., 1996, Alteration of a komatiite flow from Alexo, Ontario: *Journal Petrol*, v.37, p.1261–1284.[10.1093/petrology/37.6.1261](https://doi.org/10.1093/petrology/37.6.1261).
- Lancaster, P.J., Dey, S., Storey, C.D., Mitra, A., and Bhunia, R.K., 2015, Contrasting crustal evolution processes in the Dharwar craton: Insights from detrital zircon U–Pb and Hf isotopes: *Gondwana Research*, v.28, p.1361–1372.[10.1016/j.gr.2014.10.010](https://doi.org/10.1016/j.gr.2014.10.010).
- Le Bas, M.J.J., Maitre, R.W.L., Streckeisen, A., Zanettin, B., Le Maitre, R.W., Streckeisen, A., and Zanettin, B., 1986, A chemical classification of volcanic rocks based on the total alkali-silica diagram: *Journal Petrol*, v.27, p.745–750.[10.1093/petrology/27.3.745](https://doi.org/10.1093/petrology/27.3.745).
- Liu, S., Zhang, J., Li, Q., Zhang, L., Wang, W., and Yang, P., 2012, Geochemistry and U–Pb zircon ages of metamorphic volcanic rocks of the Paleoproterozoic Lüliang Complex and constraints on the evolution of the Trans-North China Orogen, North China Craton: *Precambrian Research*, v.222–223, p.173–190.[10.1016/j.precamres.2011.07.006](https://doi.org/10.1016/j.precamres.2011.07.006).
- Manikyamba, C., Ganguly, S., Saha, A., Santosh, M., Rajanikanta Singh, M., Subba Rao, D.V., Singh, M.R., and Rao, D.V., 2014, Continental lithospheric evolution: Constraints from the geochemistry of felsic volcanic rocks in the Dharwar Craton, India: *Journal Asian Earth Science*, v.95, p.65–80.[10.1016/j.jseaes.2014.05.015](https://doi.org/10.1016/j.jseaes.2014.05.015).
- Manikyamba, C., and Kerrich, R., 2011, Geochemistry of alkaline basalts and associated high-mg basalts from the 2.7 Ga penakacherla terrane, dharwar craton, india: An archean depleted mantle-oib array: *Precambrian Research*, v.188, p.104–122.[10.1016/j.precamres.2011.03.013](https://doi.org/10.1016/j.precamres.2011.03.013).
- Manikyamba, C., and Kerrich, R., 2012, Eastern Dharwar Craton, India: continental lithosphere growth by accretion of diverse plume and arc terranes: *Geosci Frontiers*, v.3, p.225–240.[10.1016/j.gsf.2011.11.009](https://doi.org/10.1016/j.gsf.2011.11.009).
- Manikyamba, C., Kerrich, R., Khanna, T.C., and Subba Rao, D.V., 2007, Geochemistry of adakites and rhyolites from the Neoproterozoic Gadwal greenstone belt, eastern Dharwar craton, India: Implications for sources and geodynamic setting: *Canada Journal Earth Sciences*, v.44, p.1517–1535.[10.1139/E07-034](https://doi.org/10.1139/E07-034).
- Manikyamba, C., Kerrich, R., Polat, A., Raju, K., Satyanarayanan, M., and Krishna, A.K., 2012, Arc picrite-potassic adakitic-shoshonitic volcanic association of the Neoproterozoic Sigegudda greenstone terrane, western Dharwar craton: Transition from arc wedge to lithosphere melting: *Precambrian Research*, v.212–213, p.207–224.[10.1016/j.precamres.2012.05.006](https://doi.org/10.1016/j.precamres.2012.05.006).
- Manikyamba, C., Naqvi, S.M., Subba Rao, D.V., Ram Mohan, M., Khanna, T.C., Rao, T.G., and Reddy, G.L.N., 2005, Boninites from the neoproterozoic gadwal greenstone belt, Eastern Dharwar Craton, India: implications for Archaean subduction processes: *Earth and Planetary Science Letters*, v.230, p.65–83.[10.1016/j.epsl.2004.06.023](https://doi.org/10.1016/j.epsl.2004.06.023).
- Maruyama, S., Hasegawa, A., Santosh, M., Kogiso, T., Omori, S., Nakamura, H., Kawai, K., and Zhao, D., 2009, The dynamics of big mantle wedge, magma factory, and metamorphic-metasomatic factory in subduction zones: *Gondwana Research*, v.16, p.414–430.[10.1016/j.gr.2009.07.002](https://doi.org/10.1016/j.gr.2009.07.002).
- Maury, R.C., Defant, M.J., and Joron, J.-L., 1992, Metasomatism of the sub-arc mantle inferred from trace elements in Philippine xenoliths: *Nature*, v.360, p.661–663.[10.1038/360661a0](https://doi.org/10.1038/360661a0).
- McCulloch, M.T., and Gamble, J.A., 1991, Geochemical and geodynamical constraints on subduction zone magmatism: *Earth and Planetary Science Letters*, v.102, p.358–374.[10.1016/0012-821X\(91\)90029-H](https://doi.org/10.1016/0012-821X(91)90029-H).
- McKenzie, D., 1989, Some remarks on the movement of small melt fractions in the mantle: *Earth and Planetary Science Letters*, v. 95, p. 53–72.
- McKenzie, D., and Bickle, M.J., 1988, The volume and composition of melt generated by extension of the lithosphere: *Journal Petrol*, v.29, p.625–679.[10.1093/petrology/29.3.625](https://doi.org/10.1093/petrology/29.3.625).
- McKenzie, D.A.N., and O’Nions, R.K., 1991, Partial melt distributions from inversion of rare earth element concentrations: *Journal Petrol*, v.32, p.1021–1091.[10.1093/petrology/32.5.1021](https://doi.org/10.1093/petrology/32.5.1021).
- Naqvi, S.M., Khan, R.M.K., Manikyamba, C., Mohan, M.R., and Khanna, T.C., 2006, Geochemistry of the NeoArchaean high-Mg basalts, boninites and adakites from the Kushtagi-Hungund greenstone belt of the Eastern Dharwar Craton (EDC); implications for the tectonic setting: *Journal of Asian Earth Sciences*, v.27, p.25–44.[10.1016/j.jseaes.2005.01.006](https://doi.org/10.1016/j.jseaes.2005.01.006).
- Naqvi, S.M., Manikyamba, C., Rao, T.G., Rao, D.V.S., Mohan, M. R., and Sarma, D.S., 2002, Geochemical and isotopic constraints of neoproterozoic fossil plume for evolution of volcanic rocks of sandur greenstone belt, India: *Journal of Geological Society of India*, v. 60, p. 27–56.
- Naqvi, S.M., Ram Mohan, M., Rana Prathap, J.G., and Srinivasa Sarma, D., 2009, Adakite-TTG connection and fate of mesoproterozoic basaltic crust of holenarsipur nucleus, Dharwar Craton, India: *Journal Asian Earth Science*, v.35, p.416–434.[10.1016/j.jseaes.2009.02.005](https://doi.org/10.1016/j.jseaes.2009.02.005).
- Nesbitt, H.W., and Young, G.M., 1982, Early Proterozoic climates and plate motions inferred from major element chemistry of lutites: *Nature*, v.299, p.715–717.[10.1038/299715a0](https://doi.org/10.1038/299715a0).
- Nutman, A.P., Chadwick, B., Krishna Rao, B., and Vasudev, V.N., 1996, SHRIMP U/Pb zircon ages of acid volcanic rocks in the Chitradurga and Sandur groups, and granites adjacent to the Sandur Schist belt, Karnataka: *Journal of Geological Society of India*, v. 47, p. 153–164.
- Ohtani, E., Kawabe, I., Moriyama, J., and Nagata, Y., 1989, Partitioning of elements between majorite garnet and melt and implications for petrogenesis of komatiites: *Contributions to Mineral Petrol*, v.103, p.263–269.[10.1007/BF00402913](https://doi.org/10.1007/BF00402913).

- Pearce, A.J., Barker, F.P., Edwards, J.S., Parkinson, J.I., and Leat, T.P., 2000, Geochemistry and tectonic significance of peridotites from the South Sandwich arc–basin system, South Atlantic: *Contributions to Mineral Petrol*, v.139, p.36–53. [10.1007/s004100050572](https://doi.org/10.1007/s004100050572).
- Pearce, J.A., 2008, Geochemical fingerprinting of oceanic basalts with applications to ophiolite classification and the search for Archean oceanic crust: *Lithos*, v.100, p.14–48. [10.1016/j.lithos.2007.06.016](https://doi.org/10.1016/j.lithos.2007.06.016).
- Pearce, J.A., and Peate, D.W., 1995, tectonic implications of the composition of volcanic ARC magmas: *Annual Reviews Earth Planet Sciences*, v.23, p.251–285. [10.1146/annurev.ea.23.050195.001343](https://doi.org/10.1146/annurev.ea.23.050195.001343).
- Pearce, J.A., Sieger, R., Arculus, R.C., Murton, B.J., Ishii, T., Peate, D.W., and Paerkinson, I.J., 1992, Boninite and harzburgite from leg 125 (Bonin-Mariana Forearc): A case study of magma genesis during the initial stages of subduction: *Proclam Ocean Drill Progr Results*, v. 125, p. 623–659.
- Perfit, M.R., Gust, D.A., Bence, A.E., Arculus, R.J., and Taylor, S.R., 1980, Chemical characteristics of island-arc basalts: implications for mantle sources: *Chemical Geology*, v.30, p.227–256. [10.1016/0009-2541\(80\)90107-2](https://doi.org/10.1016/0009-2541(80)90107-2).
- Peucat, -J.-J., Jayananda, M., Chardon, D., Capdevila, R., Fanning, C.M., and Paquette, J.-L., 2013, The lower crust of the Dharwar Craton, Southern India: Patchwork of Archean granulitic domains: *Precambrian Research*, v.227, p.4–28. [10.1016/j.precamres.2012.06.009](https://doi.org/10.1016/j.precamres.2012.06.009).
- Peucat, J.J., Mahabaleswar, B., and Jayananda, M., 1993, Age of younger tonalitic magmatism and granulitic metamorphism in the South Indian transition zone (Krishnagiri area); comparison with older Peninsular gneisses from the gorur? Hassan area: *Journal Metamorph Geological*, v.11, p.879–888. [10.1111/jmg.1993.11.issue-6](https://doi.org/10.1111/jmg.1993.11.issue-6).
- Polat, A., Hofmann, A., and Rosing, M., 2002, Boninite-like volcanic rocks in the 3.7–3.8 Ga Isua greenstone belt, West Greenland: Geochemical evidence for intra-oceanic subduction zone processes in the early Earth: *Chemical Geology*, v.184, p.231–254. [10.1016/S0009-2541\(01\)00363-1](https://doi.org/10.1016/S0009-2541(01)00363-1).
- Polat, A., and Kerrich, R., 2000, Archean greenstone belt magmatism and the continental growth-mantle evolution connection: Constraints from Th–U–Nb–LREE systematics of the 2.7 Ga Wawa subprovince, Superior province, Canada. *Earth and Planetary Science Letters*, v. 175, p. 41–54.
- Polat, A., and Kerrich, R., 2006, Reading the geochemical fingerprints of archaic hot subduction volcanic rocks: evidence for accretion and crustal recycling in a mobile tectonic regime, *Archean geodynamics and environments*: Washington, DC, American Geophysical Union, p. 189–213.
- Polat, A., Kerrich, R., and Wyman, D.A., 1998, The late Archean Schreiber–Hemlo and White River–Dayohessarah greenstone belts, Superior Province: Collages of oceanic plateaus, oceanic arcs, and subduction–accretion complexes: *Tectonophysics*, v.289, p.295–326. [10.1016/S0040-1951\(98\)00002-X](https://doi.org/10.1016/S0040-1951(98)00002-X).
- Rajamani, V., Shivkumar, K., Hanson, G.N., and Shirey, S.B., 1985, Geochemistry and petrogenesis of amphibolites, kolar schist belt, South India: evidence for komatiitic magma derived by low percentages of melting of the mantle: *Journal Petrol*, v.26, p.92–123. [10.1093/petrology/26.1.92](https://doi.org/10.1093/petrology/26.1.92).
- Rama Rao, B., 1962, A hand book of the geology of Mysore State, southern India, Bangalore Printing and Publishing Co., Bangalore.
- Ramachandra, H.M., 2016, Dharwar Craton - a review of regional geology and related evolutionary features: *Indian Journal Geoscience*, v. 70, p. 1–16.
- Ramakrishnan, M., and Harinadha Babu, P., 1981, Western Ghats Belt, Swami Nath, J., and Ramakrishnan, M., Eds., Early precambrian supracrustals of Southern Karnataka: Calcutta, Geological Survey of India, 147–161.
- Ramakrishnan, M., and Vaidyanadhan, R., 2010, *Geology of India*, volume 1. ed.: Bangalore, Geological Society of India.
- Rao, D.V.S., and Naqvi, S.M., 1999, Archean komatiites from the older schist belt of kalyadi in Western Dharwar Craton, Karnataka: *Journal of Geological Society of India*, v. 53, p. 347–354.
- Ross, P.S., and Bédard, J.H., 2009, Magmatic affinity of modern and ancient subalkaline volcanic rocks determined from trace-element discriminant diagrams: *Canadian Journal of Earth Sciences*, v. 46 (11), p. 823–839, [10.1139/E09-054](https://doi.org/10.1139/E09-054)
- Rudnick, R.L., and Gao, S., 2003, Composition of the Continental Crust, *Treatise on Geochemistry*.
- Rudnick, R.L., and Gao, S., 2014, Composition of the continental crust, *Treatise on Geochemistry*, Amsterdam, Elsevier, 1–51.
- Rudnick, R.L.R.L., and Fountain, D.M.D.M., 1995, Nature and composition of the continental crust - a lower crustal perspective: *Reviews Geophys*, v.33, p.267–309. [10.1029/95RG01302](https://doi.org/10.1029/95RG01302).
- Said, N., Kerrich, R., Cassidy, K., and Champion, D.C., 2012, Characteristics and geodynamic setting of the 2.7 Ga Yilgarn heterogeneous plume and its interaction with continental lithosphere: Evidence from komatiitic-basalt and basalt geochemistry of the Eastern Goldfields Superterrane. *Aust: Journal Earth Sciences*, v. 59, p. 1–27.
- Sampat Iyengar, P., 1912, The geology of Kudremukh and Gangamula regions, Kadur district: Record Mysore Geological Department, v. 12, p. 45–70.
- Saunders, A.D., Storey, M., Kent, R.W., and Norry, M.J., 1992, Consequences of plume-lithosphere interactions, Storey, B. C., Alabaster, T., and Pankhurst, R.J., Eds., *Magmatism and the cause of continental breakup*, Geological Society of London (Special Publication 68), London, 41–60.
- Sheraton, J.W., Black, L.P., McCulloch, M.T., and Oliver, R.L., 1990, Age and origin of a compositionally varied mafic dyke swarm in the Bunge Hills, East Antarctica: *Chemical Geology*, v.85, p.215–246. [10.1016/0009-2541\(90\)90002-O](https://doi.org/10.1016/0009-2541(90)90002-O).
- Smithies, R.H., 2002, Archean boninite-like rocks in an intracratonic setting: *Earth and Planetary Science Letters*, v.197, p.19–34. [10.1016/S0012-821X\(02\)00464-8](https://doi.org/10.1016/S0012-821X(02)00464-8).
- Song, X.-Y., Qi, H.-W., Robinson, P.T., Zhou, M.-F., Cao, Z.-M., and Chen, L.-M., 2008, Melting of the subcontinental lithospheric mantle by the Emeishan mantle plume; evidence from the basal alkaline basalts in Dongchuan, Yunan, Southwestern China: *Lithos*, v.100, p.93–111. [10.1016/j.lithos.2007.06.023](https://doi.org/10.1016/j.lithos.2007.06.023).
- Sproule, R.A., Leshner, C.M., Ayer, J.A., Thurston, P.C., and Herzberg, C.T., 2002, No Title Spatial and temporal variations in the geochemistry of komatiites and komatiitic basalts in the Abitibi greenstone belt: *Precambrian Research*, v.115, p.153–186. [10.1016/S0301-9268\(02\)00009-8](https://doi.org/10.1016/S0301-9268(02)00009-8).
- Srikantia, S.V., and Bose, S.S., 1985, archaic komatiites from banasandra area of kibbanahalli arm of chitradurga supra-crustal belt in Karnataka: *Journal of Geological Society of India*, v. 26, p. 407–417.

- Srikantia, S.V., and Venkataramana, P., 1989, the archaean komatiites of nagamangala supracrustal belt, Karnataka: *Journal of Geological Society of India*, v. 33, p. 210–214.
- Stern, R.J., Morris, J., Bloomer, S.H., and Hawkins, J.W., 1991, The source of the subduction component in convergent margin magmas: Trace element and radiogenic isotope evidence from Eocene boninites, Mariana forearc: *Geochimica Et Cosmochimica Acta*, v.55, p.1467–1481.[10.1016/0016-7037\(91\)90321-U](https://doi.org/10.1016/0016-7037(91)90321-U).
- Sun, -S.-S., and McDonough, W.F., 1989, Chemical and isotopic systematics of oceanic basalts: Implications for mantle composition and processes, Saunders, A.D., and Norry, M.J., Eds., *Magma-tism in oceanic basins*, Geological Society of London (Special Publication), London, 313–345.
- Sun, -S.-S., and Nesbitt, R.W., 1978, Petrogenesis of Archaean ultrabasic and basic volcanism: Evidence from rare earth elements: *Contributions to Mineral Petrol*, v.65, p.301–325.[10.1007/BF00375516](https://doi.org/10.1007/BF00375516).
- Swami Nath, J., and Ramakrishnan, M., 1981, The early pre-cambrian supracrustals of Southern Karnataka: *Geological Society of India Memoir*, v. 112, p. 350.
- Swami Nath, J., Ramakrishnan, M., Viswanatha, M.N., Ramakrishnan, M., and Viswanatha, M.N.N., 1976, Dharwar stratigraphic model and Karnataka craton evolution: *Geological Survey India Record*, v. 107, p. 149–175.
- Sylvester, P.J., Campbell, I.H., and Bowyer, D.A., 1997, Niobium/ Uranium evidence for early formation of continental crust: *Science* (80-), v.275, p.521–523.[10.1126/science.275.5299.521](https://doi.org/10.1126/science.275.5299.521).
- Tang, D.-M., Qin, K.-Z., Sun, H., Su, B.-X., and Xiao, Q.-H., 2012, The role of crustal contamination in the formation of Ni–Cu sulfide deposits in Eastern Tianshan, Xinjiang, Northwest China: Evidence from trace element geochemistry, Re–Os, Sr–Nd, zircon Hf–O, and sulfur isotopes: *Journal Asian Earth Science*, v.49, p.145–160.[10.1016/j.jseas.2011.11.014](https://doi.org/10.1016/j.jseas.2011.11.014).
- Tatsumi, Y., and Maruyama, S., 1989, Boninites and high-Mg andesites: Tectonics and petrogenesis, Crawford, A.J., Ed., *Boninites*: London, Unwin Hyman, p. 50–71.
- Taylor, S.R., and McLennan, S.M., 1985, The continental crust: its composition and evolution, an examination of the geochemical record preserved in sedimentary rocks, Blackwell, London.
- Thompson, R.N., and Morrison, M.A., 1988, Asthenospheric and lower-lithospheric mantle contributions to continental extensional magmatism: An example from the British Tertiary Province: *Chemical Geology*, v.68, p.1–15.[10.1016/0009-2541\(88\)90082-4](https://doi.org/10.1016/0009-2541(88)90082-4).
- Ugarkar, A.G., Chandan Kumar, B., and Manuvachari, T.B., 2014, Geology and geochemistry of archaean metavolcanic rocks of the northern part of the dharwar-shimoga greenstone belt, Dharwar Craton, India: implications for their petrogenesis and geodynamic setting: *Indian Mineral*, v. 48, p. 88–107.
- Ugarkar, A.G., Malapur, M.A., and Chandan Kumar, B., 2016, Archean turbidite hosted orogenic gold mineralization in the gadag greenstone belt, Western Dharwar Craton, Peninsular India: *Ore Geology Reviews*, v.72, p.1224–1242.[10.1016/j.oregeorev.2015.06.020](https://doi.org/10.1016/j.oregeorev.2015.06.020).
- Ugarkar, A.G., Solankar, S.N., and Vasudev, V.N., 2013, Geology and geochemistry of archaean felsic metavolcanic rocks of the Eastern Part of the kolar greenstone belt, Dharwar craton, India: Implications for their petrogenesis and geodynamic setting: *Journal of Geological Society of India*, v.81, p.192–202.[10.1007/s12594-013-0022-x](https://doi.org/10.1007/s12594-013-0022-x).
- Viljoen, M.J., Viljoen, F.P., and Pearton, T.N., 1982, the nature and distribution of archaean komatiite volcanics in South Africa, Arndt, N.T., and Nisbet, E.G., Eds., *Komatiites*, Allen and Unwin, London, 53–79.
- Viswanatha, M.N., Ramakrishnan, M., and Kutty, T.R.N., 1977, Possible Spinifex Texture in a Serpentinite from Karnataka: *Journal of Geological Society of India*, v. 18, p. 194–197.
- Winchester, J.A., and Floyd, P.A., 1977, Geochemical discrimination of different magmaseries and their differentiation products using immobile elements: *Chemical Geology*, v.20, p.325–343.[10.1016/0009-2541\(77\)90057-2](https://doi.org/10.1016/0009-2541(77)90057-2).
- Windley, B.F., 1993, Uniformitarianism today: Plate tectonics is the key to the past: *Journal of Geological Society of London*, v.150, p.7–19.[10.1144/gsjgs.150.1.0007](https://doi.org/10.1144/gsjgs.150.1.0007).
- Zhao, J.-H., and Zhou, M.-F., 2007, Geochemistry of Neoproterozoic mafic intrusions in the Panzhihua district (Sichuan Province, SW China): Implications for subduction-related metasomatism in the upper mantle: *Precambrian Research*, v.152, p.27–47.[10.1016/j.precamres.2006.09.002](https://doi.org/10.1016/j.precamres.2006.09.002).
- Zhao, J.-X., Shiraishi, K., Ellis, D.J., and Sheraton, J.W., 1995, Geochemical and isotopic studies of syenites from the Yamato Mountains, East Antarctica: Implications for the origin of syenitic magmas: *Geochimica Et Cosmochimica Acta*, v.59, p.1363–1382.[10.1016/0016-7037\(95\)00050-A](https://doi.org/10.1016/0016-7037(95)00050-A).
- Zhou, M.-F., Robinson, P.T., Su, B.-X., Gao, J.-F., Li, J.-W., Yang, J.-S., and Malpas, J., 2014, Compositions of chromite, associated minerals, and parental magmas of podiform chromite deposits: the role of slab contamination of asthenospheric melts in suprasubduction zone environments: *Gondwana Research*, v.26, p.262–283.[10.1016/j.gr.2013.12.011](https://doi.org/10.1016/j.gr.2013.12.011).